AD-A036 026 AUBURN UNIV ALA ENGINEERING EXPERIMENT STATION F/G 11/4
TECHNIQUES FOR FLAW DETECTION IN COMPOSITE MATERIAL STRUCTURES.(U)
DEC 76 W F RANSON, W F SWINSON DAAH01-76-C-0467
UNCLASSIFIED ME-AMC-0467 NL

| OF |
AD
A036026

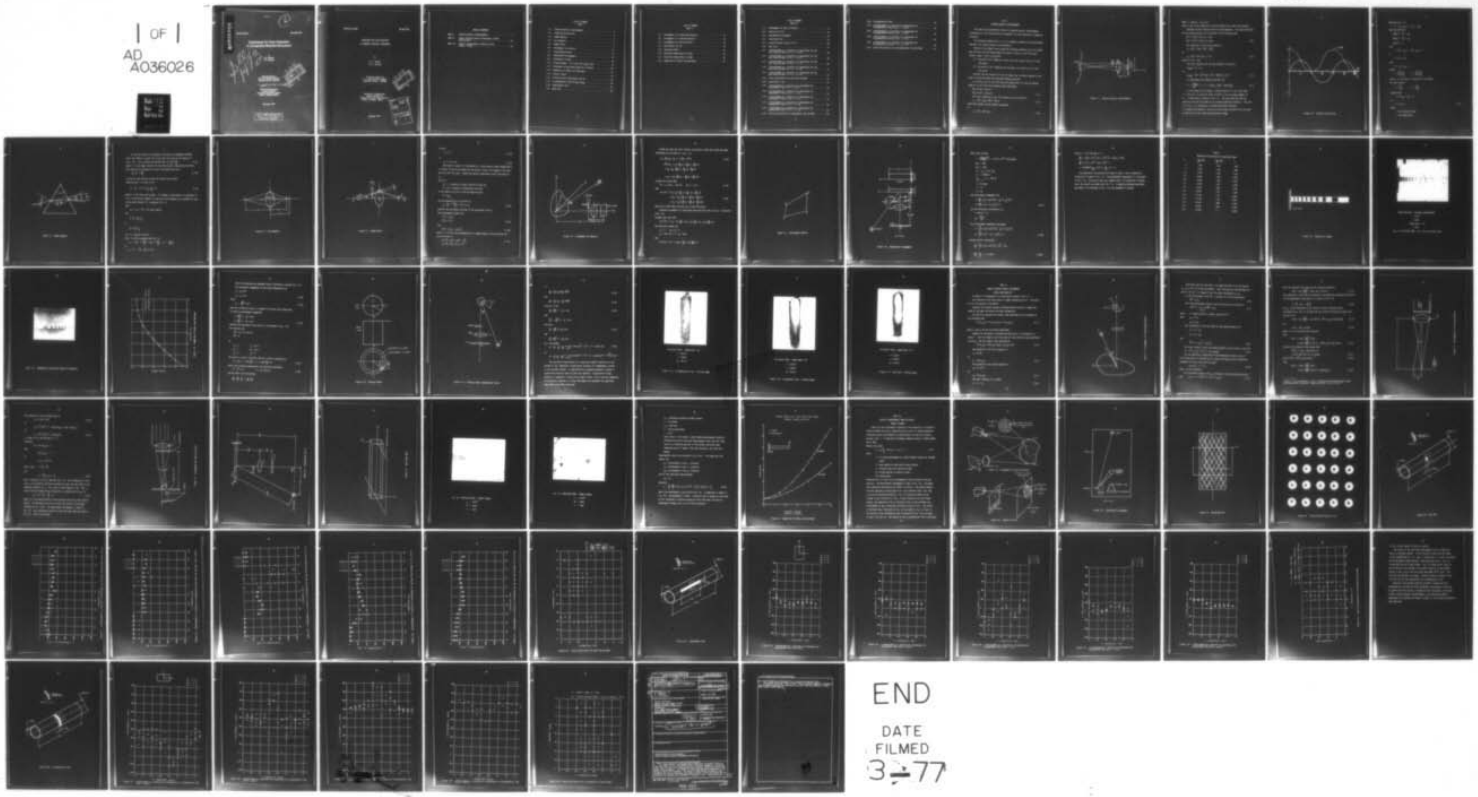

END

DATE
FILMED
3-77


1.0
1.1
1.25
1.4
1.6
1.8
2.0
2.2
2.5
2.8
3.2
3.6
4.0
4.5
5.0
5.6
MICROCOPY RESOLUTION TEST CHART
NATIONAL BUREAU OF STANDARDS-1963

Technical Report

ME-AMC 0467

Techniques for Flaw Detection in Composite Material Structures

by
W.F. Ranson
W.F. Swinson

Technical Report to
U.S. Army Missile Command
Redstone Arsenal, Alabama

DAAH 01-76-C-0467

Mechanical Engineering
Auburn University
Engineering Experiment Station
Auburn, Alabama 36830

December 1976

TECHNICAL REPORT

ME-AMC 0467

TECHNIQUES FOR FLAW DETECTION IN COMPOSITE MATERIAL STRUCTURES

by

W. F. Ranson
W. F. Swinson

Technical Report to
U. S. Army Missile Command
Redstone Arsenal, Alabama

Mechanical Engineering
Auburn University
Engineering Experiment Station
Auburn, Alabama 36830

December 1976

TABLE OF CONTENTS

LIST OF FIGURES
PART I

LIST OF FIGURES
PART II

LIST OF FIGURES
PART III

Part I

SHEARING SPECKLE INTERFEROMETRY

The theory and experimental results of shearing speckle interferometry are presented in this section with its potential for flaw detection in composite cylinders.

The following diagram (Fig. 1.1) is a schematic diagram of the experimental apparatus for shearing speckle interferometry.

Because of the wedge in the system the following conditions will be formed when the lens plus the wedge images the points P and P_1 on the film plane. Assume a shear in the +x direction.

(1) The point P will image at a point (x,y) and a point $(X+\Delta_i, y)$ in the film plane.

(2) The point P_1 will image due to the shear, at a point (x,y) in the film plane.

Consider now the intensity of the two images due to double exposure of the plate in which the object was deformed between exposures.

At a point (x,y) in the film plane the image point of P and the sheared image of P_1 will have the following light amplitudes.

$$\bar{E}p = \bar{A} \exp i\, \theta p(x,y)$$

$$\bar{E}p_1 = \bar{A} \exp i\, \theta p_1(x,y) \qquad (1.1)$$

The total intensity of the first exposure can be written as

$$I_1 = (\bar{E}p + \bar{E}p_1) \cdot (\bar{E}p^* + \bar{E}p_1^*) \qquad (1.2)$$

where $\bar{E}p^*$ and $\bar{E}p_1^*$ denote complex conjugates,

or

$$I_1 = 2A^2 + 2A^2 \cos \theta \qquad (1.3)$$

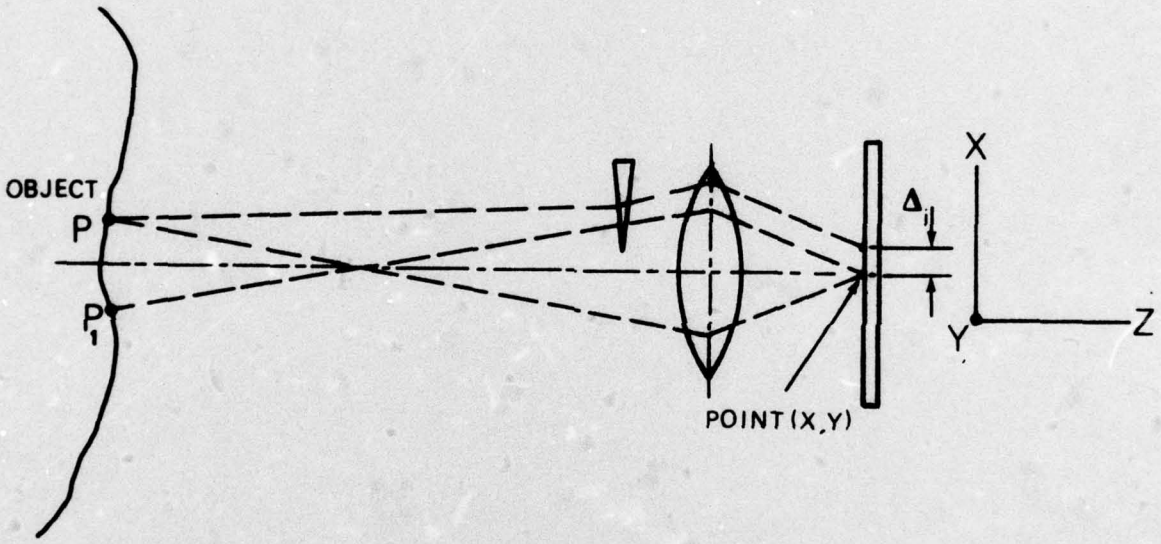

Figure 1-1. Shearing Speckle Interferometry

where $\Theta = \theta p(x,y) - \theta p_1 (x,y)$

where I_1 now is the intensity at the film plane due to the first exposure.

Consider now the intensity for the second exposure. The light amplitudes for the second exposure can be written in the following form

$$\bar{E}p' = \bar{A} \exp i (\theta p(x,y) + \Delta\theta p)$$

$$\bar{E}p_1' = \bar{A} \exp i (\theta p_1(x,y) + \Delta\theta p_1) \qquad (1.4)$$

The intensity of the second exposure is

$$I_2 = (\bar{E}p' + \bar{E}p_1') \cdot (\bar{E}^*p' + \bar{E}^*p_1')$$

or

$$I_2 = 2A^2 + 2A^2 \cos (\Theta + \Delta\Theta) \qquad (1.5)$$

where $\Delta\Theta = \Delta\theta p - \Delta\theta p'$

The total intensity for the two exposures is given by

$$I_{TOTAL} = I_1 + I_2$$

or

$$I_{TOTAL} = 2A^2 + 2A^2 \cos\Theta + 2A^2 + 2A^2 \cos (\Theta + \Delta\Theta) \qquad (1.6)$$

To investigate the intensity equation let

$$I' = \frac{I_{TOTAL}}{2A^2} = 2 + (1 + \cos\Delta\Theta) \cos\Theta - \sin\Theta \sin\Delta\Theta \qquad (1.7)$$

In the formation of fringes, a relative zero of I' will occur when $(1 + \cos \Delta\Theta) = o$ since the value of $\sin \Delta\Theta = 0$ for the same argument of $\Delta\Theta$. A description is shown in Fig. 1.2. The terms $\cos\Theta$ and $\sin\Theta$ are arbitrary and will be evident as an average background intensity. The term "2" of eq. (1.7) represents a constant background intensity.

To interpret the physical meaning of the fringes consider first the shear or deviation of the light passing through a wedge.

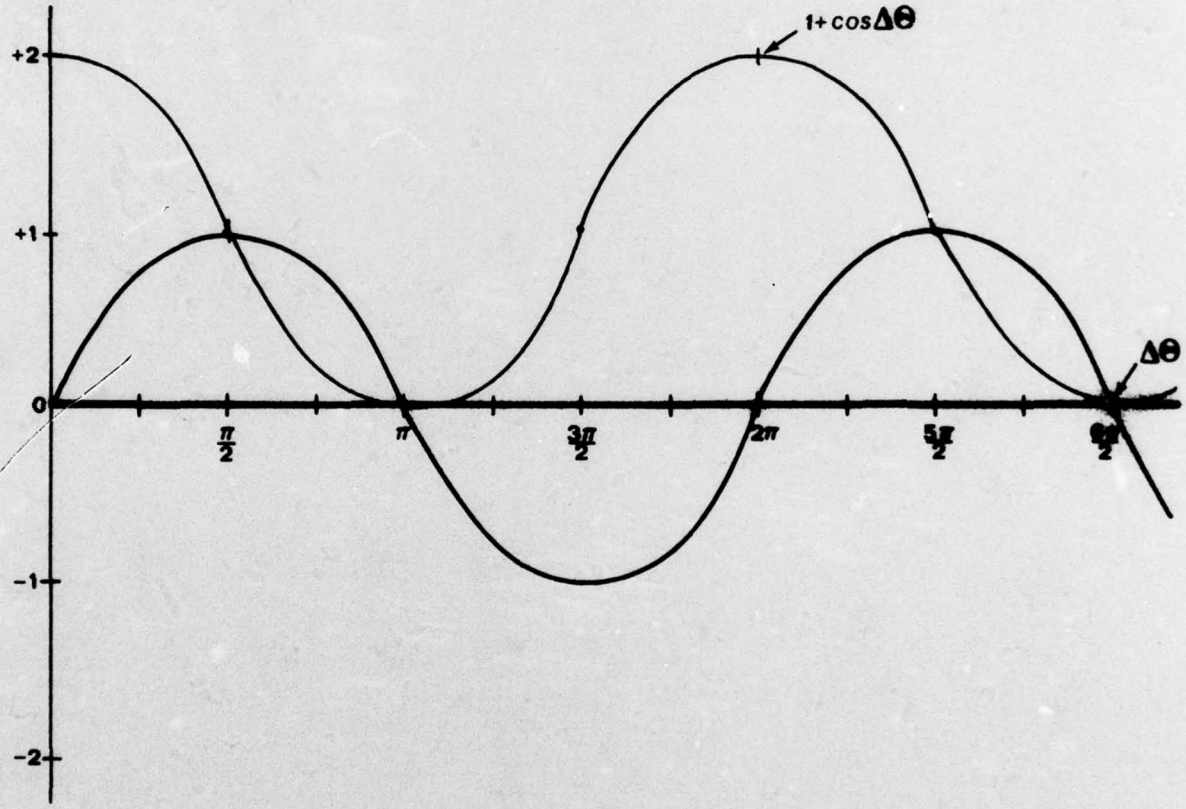

Figure 1-2. Intensity Distribution

Reference Fig. 1.3

$$\delta = (\theta_{i1} - \theta_{t1}) + (\theta_{t2} - \theta_{i2})$$

note the relations

$$\measuredangle 312 = \frac{\pi}{2} - \theta_{t1}$$

$$\measuredangle 321 = \frac{\pi}{2} - \theta_{i2}$$

$$\measuredangle 132 = \alpha$$

thus

$$\pi = (\frac{\pi}{2} - \theta_{t1}) + (\frac{\pi}{2} - \theta_{i2}) + \alpha$$

or

$$\alpha = \theta_{t1} + \theta_{i2}$$

and

$$\delta = \theta_{i1} + \theta_{t2} - \alpha$$

Recall

$$n = \frac{\sin \theta_{i1}}{\sin \theta_{t1}} \quad , \quad n = \frac{\sin \theta_{t2}}{\sin \theta_{i2}}$$

where n is the index of refraction of the wedge.

For small angles

$$n = \frac{\theta_{i1}}{\theta_{t1}} \quad , \quad n = \frac{\theta_{t2}}{\theta_{i2}}$$

Substituting

$$\delta = n (\theta_{t1} + \theta_{i2}) - \alpha$$

or

$$\delta = (n-1) \alpha \qquad (1.8)$$

where

δ = the deviation angle

α = the wedge angle

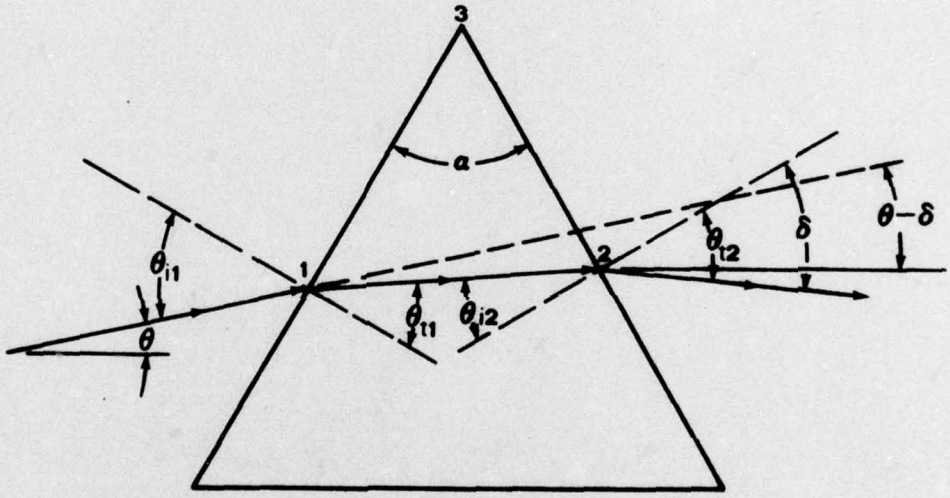

Figure 1-3. Wedge Geometry

To note the effect of the wedge on the optical arrangement consider (Thin Lens Theory) a source (s) on the lens axis that has an image at s' (Fig. 1.4). This location was derived from $\frac{1}{s} + \frac{n}{s''} = \frac{n-1}{R_1}$ (1.9) where s" is the image location for the light source intersecting the first lens surface and assuming air as the first medium and from

$$-\frac{n}{s''} + \frac{1}{s'} = \frac{1-n}{R_2} \tag{1.10}$$

for the new wave surface leaving the second lens surface.

Conbining eqs. (1.9) and (1.10)

$$\frac{1}{s} + \frac{1}{s'} = (n-1)\left(\frac{1}{R_1} - \frac{1}{R_2}\right) = \frac{1}{f} \tag{1.11}$$

where f is the lens focal length. If a wedge is positioned as illustrated in Fig. 1.5 the source "appears" to the lens to be located at s_A instead of s due to the angle change $(\theta-\delta)$, reference Fig. 1.3

note

$$s_A\,(\theta-\delta) = S(\theta) \quad \text{for small angles}$$

and

$$\frac{1}{s} + \frac{1}{s'} = \frac{1}{s_A} + \frac{1}{s'_A}$$

or

$$\frac{1}{s'} = -\frac{\delta}{\theta s} + \frac{1}{s'_A}$$

Let Δ_i = Amount of shift,

then as can be reasoned from Fig. 1.5

$$\Delta_i = (s'_A - s')\frac{OH}{s'_A} = (s'_A - s')\frac{s\theta}{s'_A} = \left(1 - \frac{s'}{s'_A}\right)s\theta$$

or

$$\Delta_i = \left(1 - \left[\frac{1}{s'} + \frac{\delta}{\theta s}\right]s'\right)s\theta$$

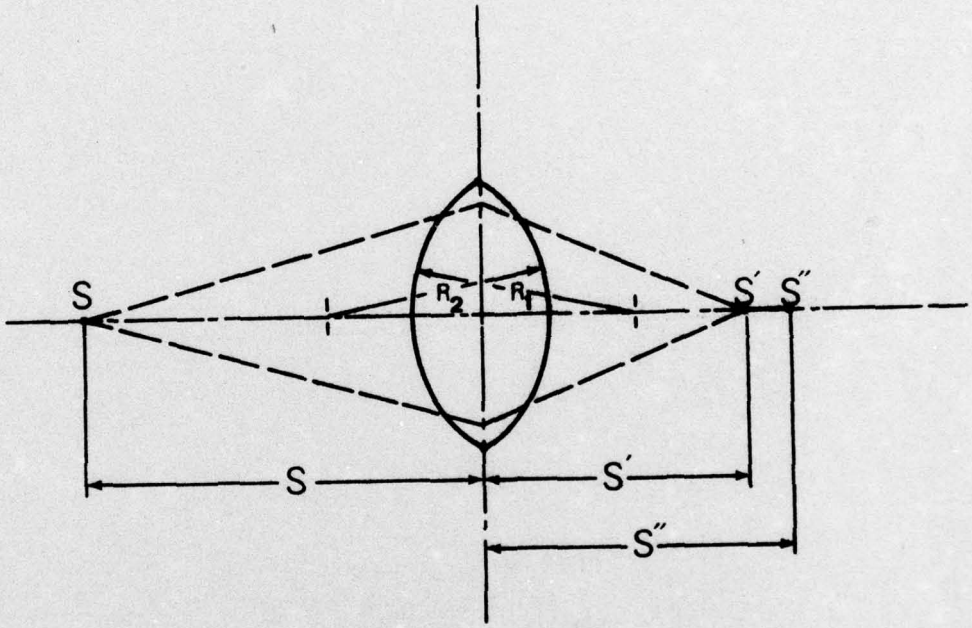

Figure 1-4. Lens Geometry

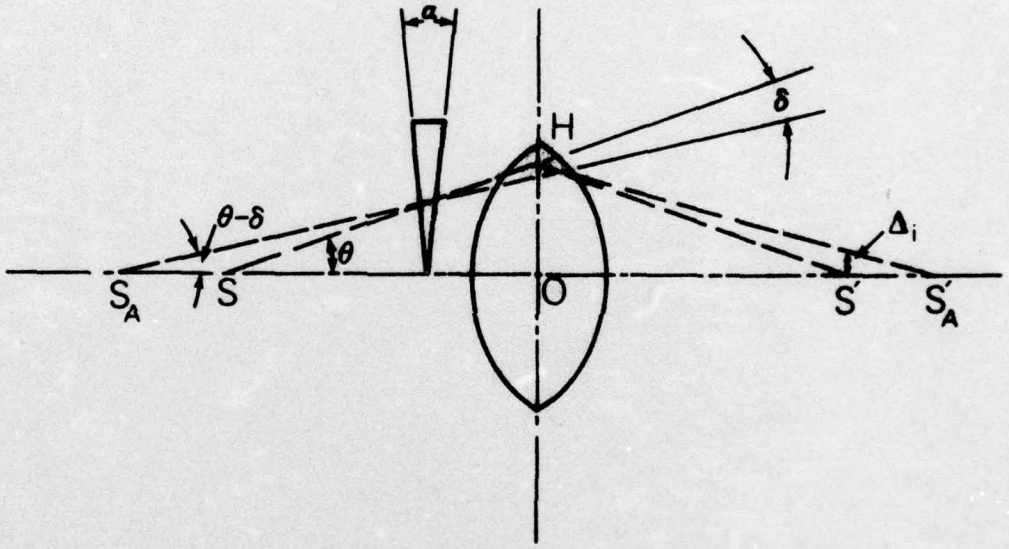

Figure 1-5. Wedge Effect

Finally

$$\Delta_i = \delta s' \tag{1.12}$$

or

$$\Delta_i = (n-1)\,\alpha s' \tag{1.13}$$

Next when an object is illuminated by a single beam as shown schematically in figure 1.6 due to the wedge the two points P and P_1 are imaged at the same point on the film plane. Denote the spatial separation on the film plane by Δ_i.

Also let

$D_o = s$ = distance of object (point P) from lens

$D_i = Dw$ = distance of image plane from lens.

If the image is not full scale the magnification

$$m = D_i/D_o$$

can be accounted for in the shift as

$$\Delta_o = \frac{\Delta_i}{m} = \frac{\Delta_i D_o}{D_i} = (n-1)\,\alpha\, D_o \tag{1.14}$$

Consider now the phase variation of the two points P and P_1.

The displacement vectors are

$$\vec{PP'} = U_i \vec{e}_i$$

$$\vec{P_1P_1'} = U_i' \vec{e}_i \tag{1.15}$$

with

$$\vec{P_1P_1'} = U_i(X_i + \Delta X_i)\,\vec{e}_i \tag{1.16}$$

when P_1 is in the close neighborhood of P. Phase change of the two points can now be written as

$$\Delta\theta_2 = \frac{2\pi}{\lambda}\,[\vec{p_1s} + \vec{p_1o}] \cdot \vec{P_1P_1} \tag{1.17}$$

$$\Delta\theta_1 = \frac{2\pi}{\lambda}\,[\vec{ps} + \vec{po}] \cdot \vec{PP'}$$

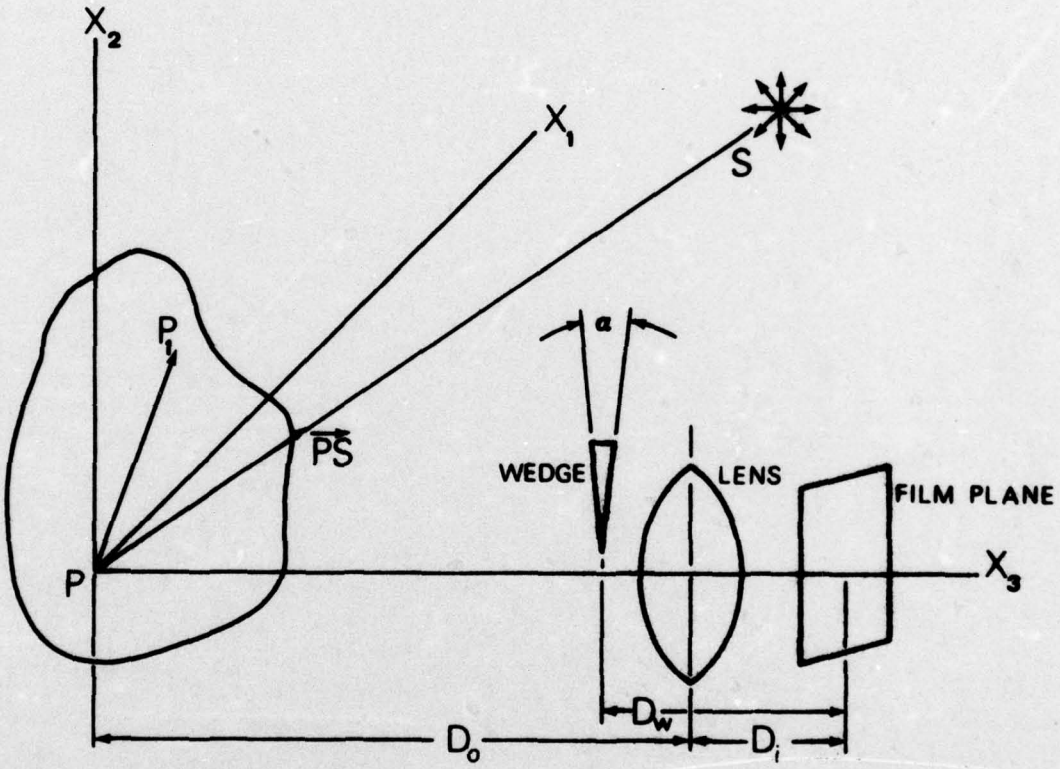

Figure 1-6. Arrangement for Analysis

Assume now that the units vectors are parallel, which now allows the phase difference to be written as (Fig. 1-7)

$$\Delta\theta = \frac{2\pi}{\lambda}[\,\bar{p}s + \bar{p}o\,]\cdot(\,\overline{P_1P_1'} - \overline{P\,P'}) \tag{1.18}$$

$$= \frac{2\pi}{\lambda}[(l_s + l_o)(\frac{\partial u}{\partial x}\Delta x + \frac{\partial u}{\partial y}\Delta y + \frac{\partial u}{\partial z}\Delta z)$$

$$+ (m_s + m_o)(\frac{\partial v}{\partial x}\Delta x + \frac{\partial v}{\partial y}\Delta y + \frac{\partial v}{\partial z}\Delta z)$$

$$+ (n_s + n_o)(\frac{\partial w}{\partial x}\Delta x + \frac{\partial w}{\partial y}\Delta y + \frac{\partial w}{\partial z}\Delta z)]$$

Fringes will occur when

$$\Delta\theta = \pi,\ 3\pi, 5\pi, \ldots (2n-1)\pi \quad \text{for } n = 1,2,\ldots \tag{1.19}$$

thus

$$(n-1/2)\lambda = [(l_s+l_o)(\frac{\partial u}{\partial x}\Delta x + \frac{\partial u}{\partial y}\Delta y + \frac{\partial u}{\partial z}\Delta z)$$

$$+ (m_s + m_o)(\frac{\partial v}{\partial x}\Delta x + \frac{\partial v}{\partial y}\Delta y + \frac{\partial v}{\partial z}\Delta z) \tag{1.20}$$

$$+ (n_s + n_o)(\frac{\partial w}{\partial x}\Delta x + \frac{\partial w}{\partial y}\Delta y + \frac{\partial w}{\partial z}\Delta z)]$$

Note that a shift does not occur out of the film plane.

Consider an example of a cantilever beam with the shift in the Z - direction (Fig. 1.8)

Fringes occur such that

$$(n-1/2)\lambda = [(l_s + l_o)\frac{\partial u}{\partial z} + (m_s + m_o)\frac{\partial v}{\partial z} + (n_s + n_o)\frac{\partial w}{\partial z}]\,\Delta z$$

The direction cosines are

$$l_o = 1 \qquad m_o = n_o = o$$

$$l_s = \cos\theta \quad m_s = o \quad n_s = \sin\theta$$

thus

$$(n-1/2)\lambda = [(\,1 + \cos\theta\,)\frac{\partial u}{\partial z} + \sin\theta\frac{\partial w}{\partial z}]\,\Delta z$$

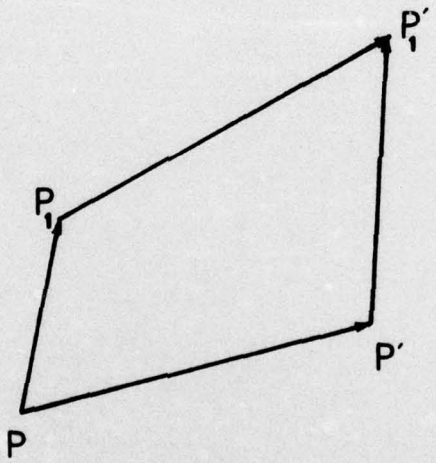

Figure 1-7. Displacement Vectors

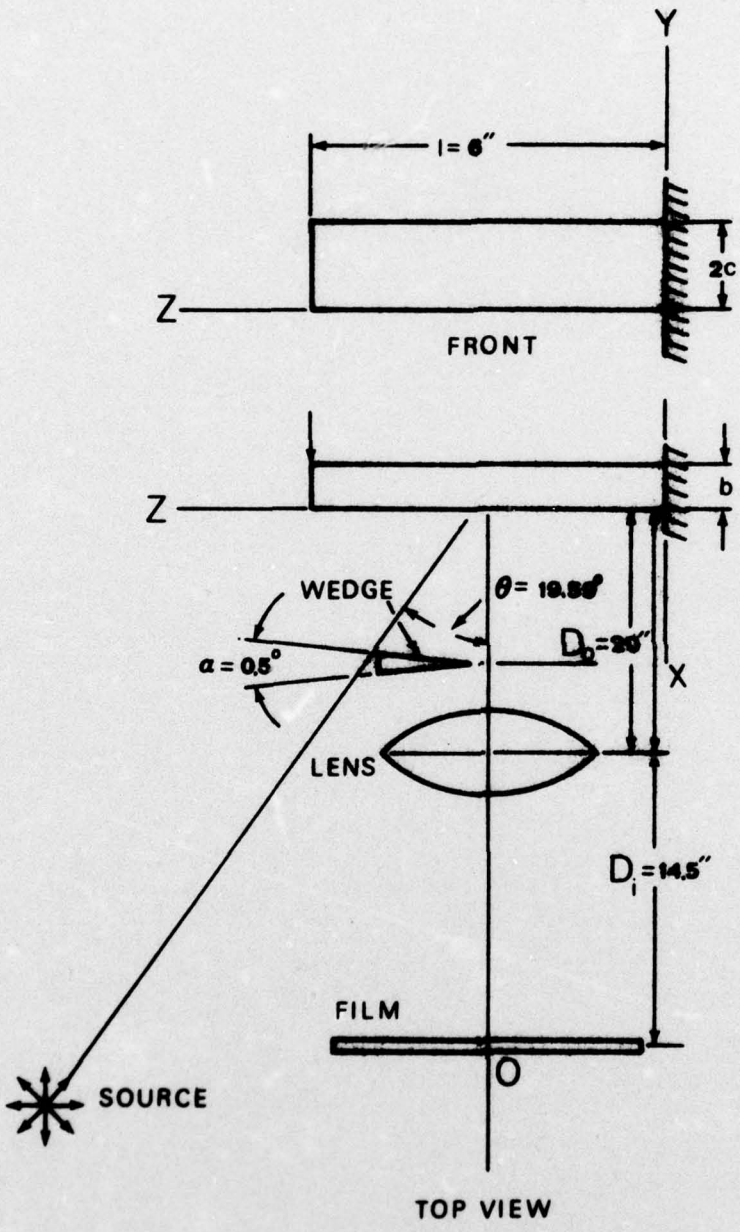

Figure 1-8. Experimental Arrangement

Other data includes

$$\lambda = \frac{6328(10^{-8})}{2.54} = 24.91 \times 10^{-6} \text{ microinches}$$

$\cos\theta = .9421$

$\sin\theta = .3353$

$\Delta z = \Delta_o = (n-1)\,\alpha D_o$

$\Delta z = 0.0899$ in

$u\big|_{x=1} = \delta_1 = .005$ in

$1 = 6$ inches

$\nu = .37$

$b = .25$

The displacement components are

$$u = \frac{Wx}{EI}\left[\frac{\nu}{2}(1-z)(x^2-y^2) - \frac{1}{6}z^3 + \frac{1}{2}1z^2\right]$$

$$w = \frac{Wx}{EI}\left[xy^2 - (1z - \frac{1}{2}z^2)\,x\right] \qquad (1.21)$$

Let the deflection be defined as δ_1,

$$u(0,0,1) = \delta_1$$

$$Wx = \frac{3EI\delta_1}{1^3}$$

The displacement components now become

$$u = \frac{3\delta_1}{1^3}\left[\frac{\nu}{2}(1-z)(x^2-y^2) - \frac{1}{6}z^3 + \frac{1}{2}1z^2\right]$$

$$w = \frac{3\delta_1}{1^3}\left[xy^2 - (1z - \frac{1}{2}z^2)\,x\right] \qquad (1.22)$$

Taking partial derivatives

$$\frac{\delta u}{\delta z} = \frac{3\delta_1}{1^3}\left[\frac{\nu}{2}(-1)(x^2-y^2) - \frac{z^2}{2} + 1z\right]$$

$$\frac{\delta w}{\delta z} = \frac{3\delta_1}{1^3}\left[-(1-z)x\right] \qquad (1.23)$$

Taking x = .125 inch and y = 0

$$\frac{\partial u}{\partial z} = -.200 \times 10^{-6} - 34.7 \times 10^{-6} z^2 + 416.4 \times 10^{-6} z$$

$$\frac{\partial w}{\partial z} = -51.6 \times 10^{-6} + 8.6 \times 10^{-6} z$$

$$n = \left[(7008.8) \frac{\partial u}{\partial z} + 1210.1 \left(\frac{\partial w}{\partial z} \right) \right] + .5$$

The theoretical calculations are shown in Table 1, and a theoretical fringe plot is shown in Fig. 1.9. The experimental photograph is illustrated in Fig. 1.10. The results were also imaged using a TV system with a Videcon tube, the results are shown with Fig. 1.11. A comparison between experiment and theory is illustrated in Fig. 1.12; the agreement is obvious.

TABLE I

Theoretical Calculation For Cantilever Beam

z	$\frac{\partial u}{\partial z}$ (10^4)	$\frac{\partial w}{\partial z}$ (10^4)	n
0	-.002	-.516	.436
.5	1.993	-.473	1.840
1.0	3.815	-.430	3.122
1.5	5.463	-.387	4.282
2.0	6.938	-.344	5.321
2.5	8.239	-.301	6.238
3.0	9.367	-.258	7.034
3.5	10.321	-.215	7.708
4.0	11.102	-.172	8.260
4.5	11.709	-.129	8.691
5.0	12.143	-.086	9.000
5.5	12.403	-.043	9.189
6.0	12.490	0	9.254

Figure 1-9. Theoretical Fringes

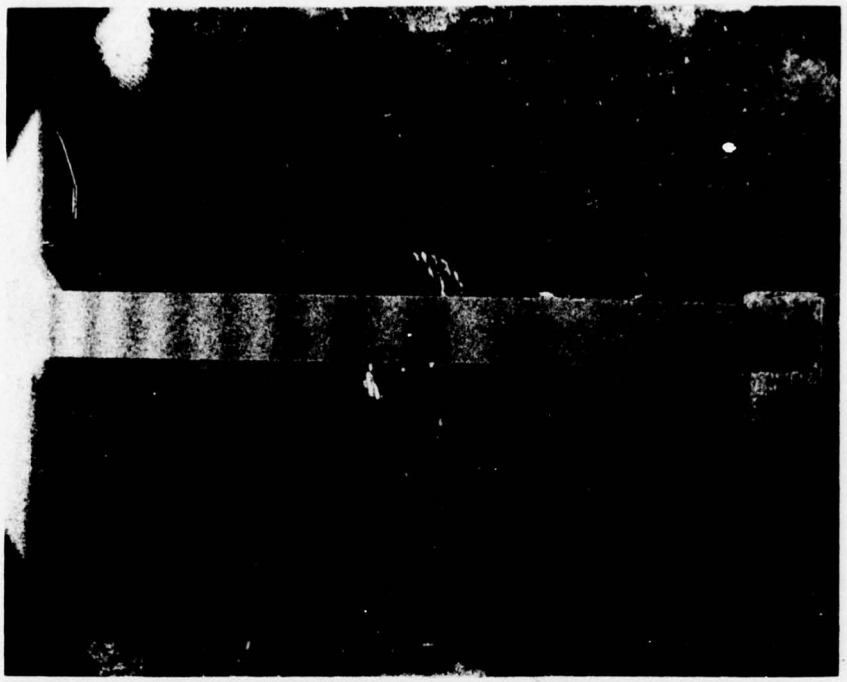

CANTILEVER BEAM - SHEARING INTERFEROMETRY

= 19.59^{o}

= 6328A

Wedge Angle - .5^{o}

= .005"

Fig. 1-10 FILTERED IMAGE - All lines with Argon Laser

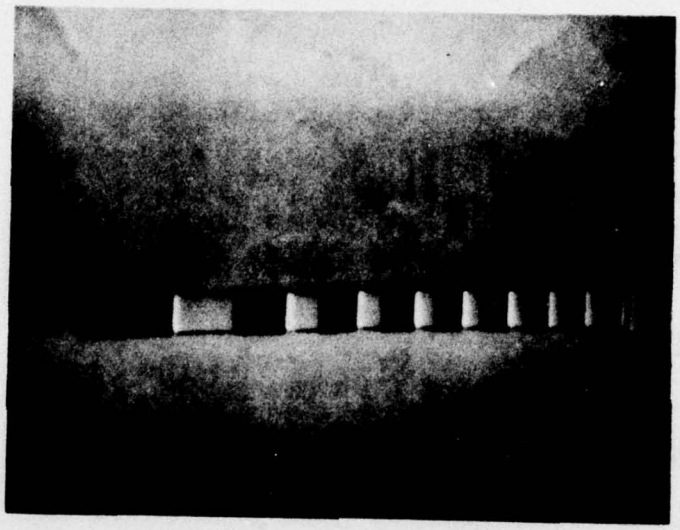

Fig. 1-11 Photograph of Cantilever Beam Off TV Monitor

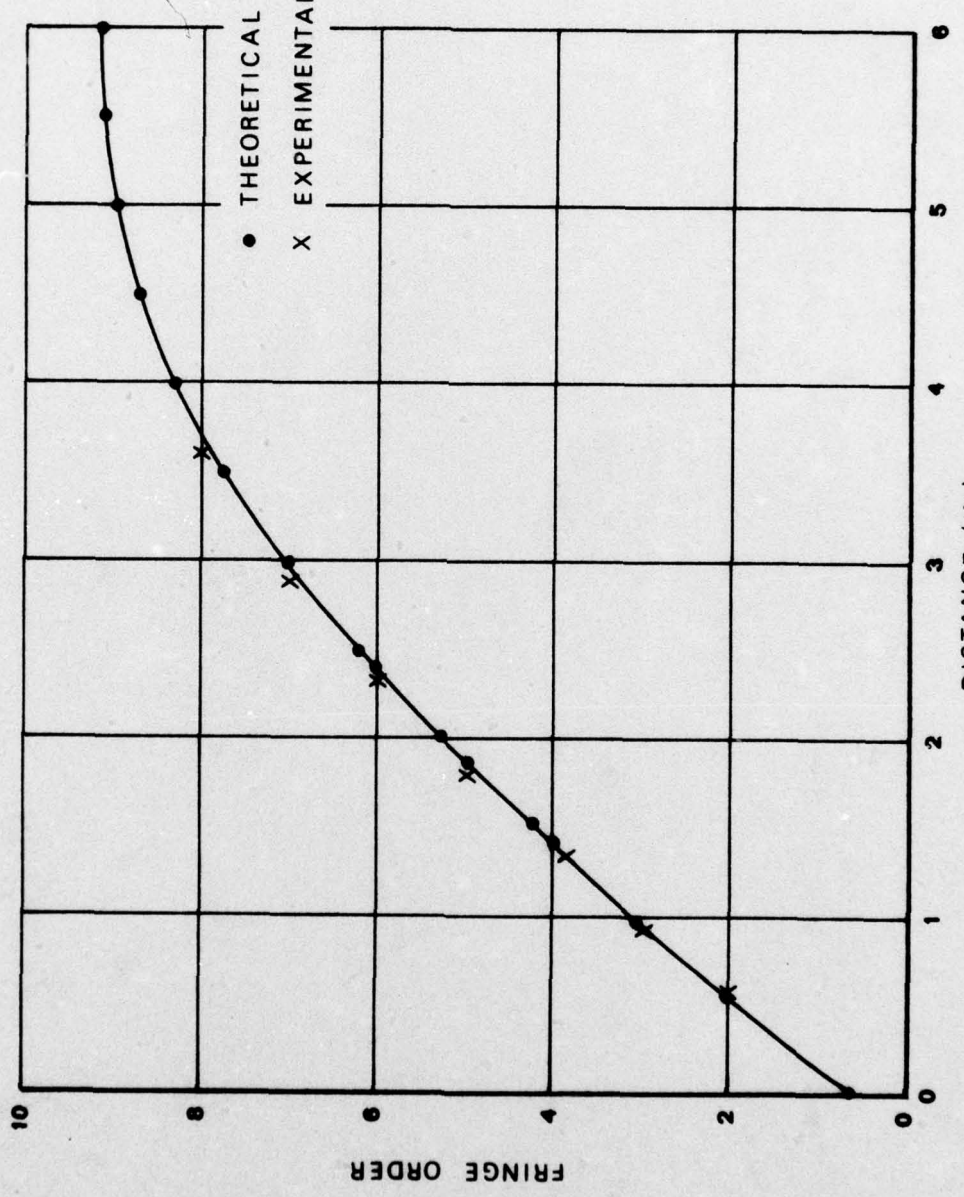

Figure 1-12. Comparison of Theory and Experiment

Next this technique was examined using a cylindrical cylinder Fig. 1.13.

The rectangular components of the radial deformation are

$$\delta_x = \delta_R \cos\theta$$

$$\delta_y = \delta_r \sin\theta \tag{1.24}$$

where

$$\delta_r = \frac{pr^2}{Et}\left(1 - \frac{\nu}{2}\right) \tag{1.25}$$

when the cylindrical vessel is assumed thin walled with capped ends.

In terms of displacement components

$$u = \frac{pr^2}{Et}\left(1 - \frac{\nu}{2}\right)\cos\theta$$

$$v = \frac{pr^2}{Et}\left(1 - \frac{\nu}{2}\right)\sin\theta \tag{1.26}$$

Consider the experiment to be set up as illustrated in Fig. 1.14.

Unit vectors are

$$\overline{ps} = \sin\beta\,\bar{i} + \cos\beta\,\bar{j}$$

$$\overline{po} = \bar{j}$$

or

$$l_o = 0 \qquad l_s = \sin\beta$$

$$m_o = 1 \qquad m_s = \cos\beta$$

$$n_o = 0 \qquad n_s = 0$$

The shift is in the x direction thus Eq. (1.20) is expressed as

$$\left(n - \frac{1}{2}\right)\lambda = \left[\sin\beta\,\frac{\partial u}{\partial x} + (1 + \cos\beta)\,\frac{\partial v}{\partial x}\right]\Delta x \tag{1.27}$$

Recall the relation between polar and cartesian coordinates

$$r^2 = x^2 + y^2 \qquad \theta = \arctan y/x \tag{1.28}$$

and the chain rule derivatives

$$\frac{\partial u}{\partial x} = \frac{\partial u}{\partial r}\,\frac{\partial r}{\partial x} + \frac{\partial u}{\partial \theta}\,\frac{\partial \theta}{\partial x}$$

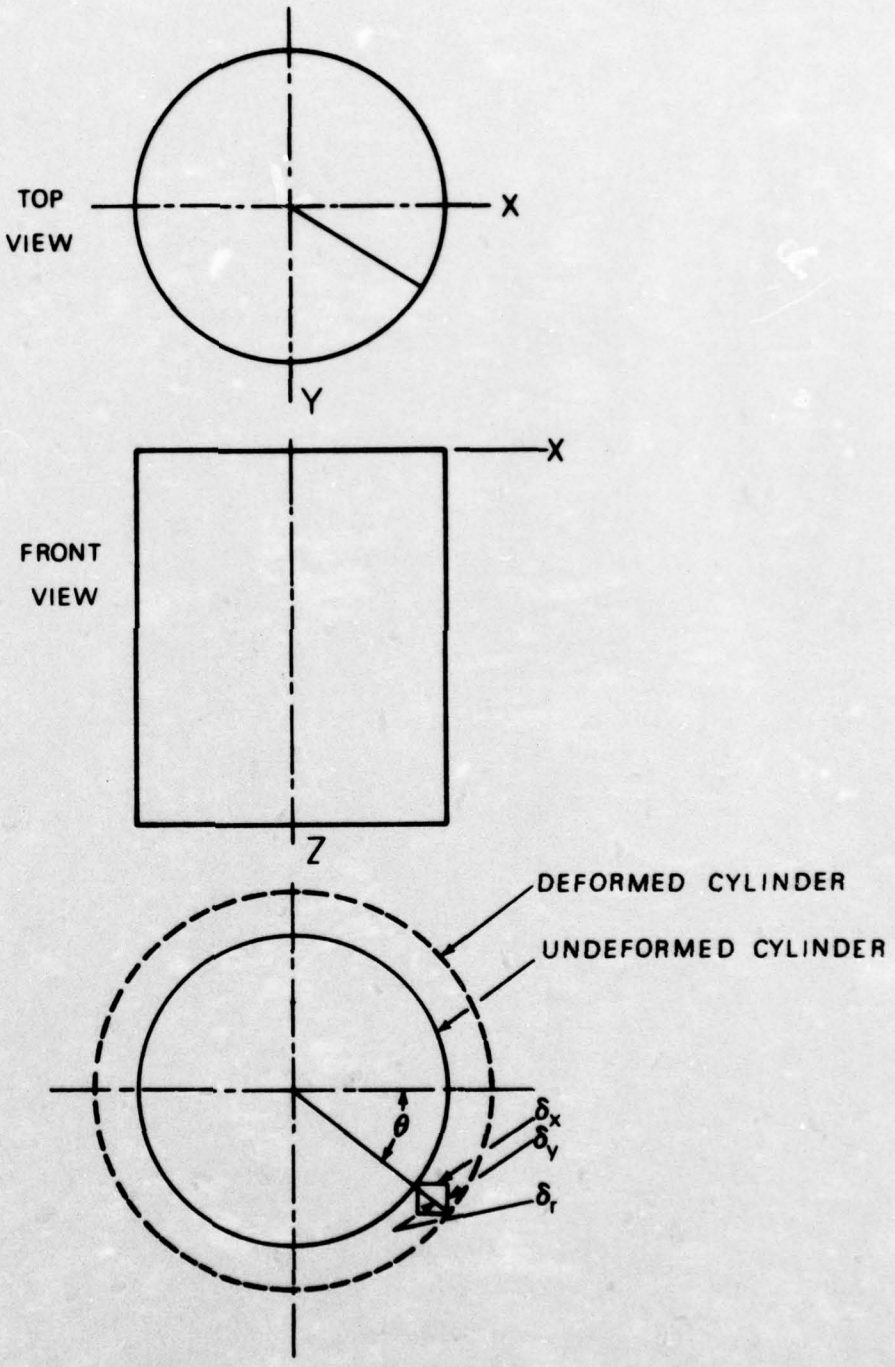

Figure 1-13. Pressure Vessel

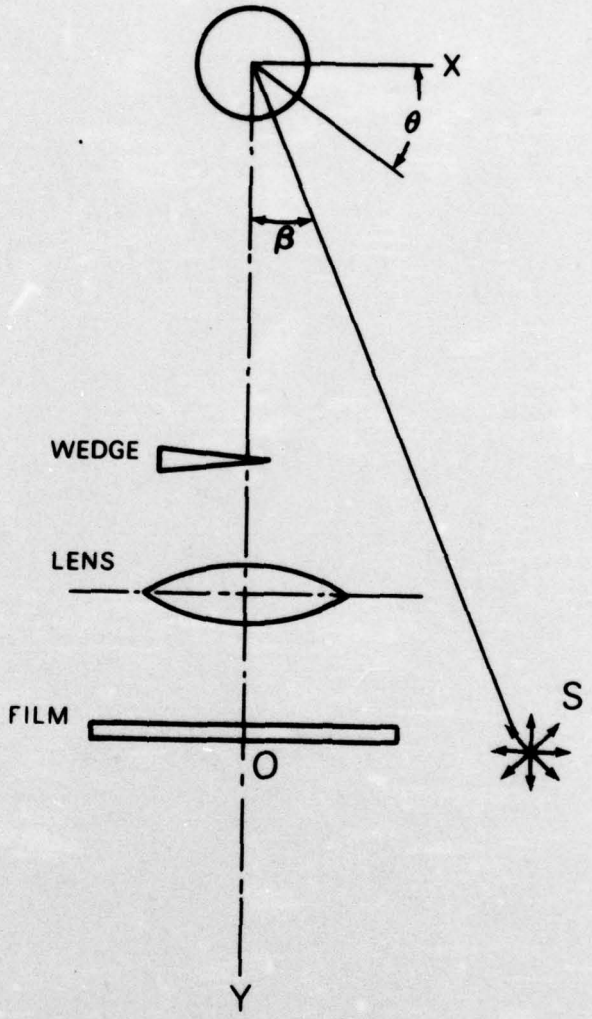

Figure 1-14. Pressure Vessel Experimental Set Up

or

$$\frac{\partial u}{\partial x} = \frac{\partial u}{\partial r}\cos\theta - \frac{\partial u}{\partial \theta}\frac{\sin\theta}{r} \tag{1.30}$$

and

$$\frac{\partial v}{\partial x} = \frac{\partial v}{\partial r}\cos\theta - \frac{\partial v}{\partial \theta}\frac{\cos\theta}{r} \tag{1.31}$$

From Eq. (1.25)

$$\frac{\partial u}{\partial r} = \frac{2pr}{Et}\left(1 - \frac{\nu}{2}\right)\cos\theta \tag{1.32}$$

and

$$\frac{\partial u}{\partial \theta} = -\frac{pr^2}{Et}\left(1 - \frac{\nu}{2}\right)\sin\theta$$

Similarly

$$\frac{\partial v}{\partial r} = \frac{2pr}{Et}\left(1 - \frac{\nu}{2}\right)\sin\theta \tag{1.33}$$

and

$$\frac{\partial v}{\partial \theta} = \frac{pr^2}{Et}\left(1 - \frac{\nu}{2}\right)\cos\theta$$

Eq. 1.26 becomes

$$\left(n - \frac{1}{2}\right)\frac{\lambda}{\Delta x} = \frac{p}{Et}\frac{\left(1 - \frac{\nu}{2}\right)}{r}\left[\sin\beta\,(2x^2 + y^2) + (1 + \cos\beta)\,xy\right] \tag{1.34}$$

or

$$\left(n - \frac{1}{2}\right)\frac{\lambda}{\Delta x} = \frac{p}{Et}\frac{\left(1 - \frac{\nu}{2}\right)}{r}\left[(\sin\beta)(x^2 + r^2) + (1 + \cos\beta)(x)(r^2 - x^2)^{\frac{1}{2}}\right] \tag{1.35}$$

The resulting fringe pattern is a relatively complex function of x and because of this complexity a quantitative analysis of a homogeneous cylinder is not straight forward. In application to a composite material cylinder a quantitative analysis would be even less feasible. A qualitative fringe pattern for composites is possible as noted in Figs. 1.15-17, but the complexity of assigning a quantity to a given flaw makes this technique less desirable than some of the other techniques.

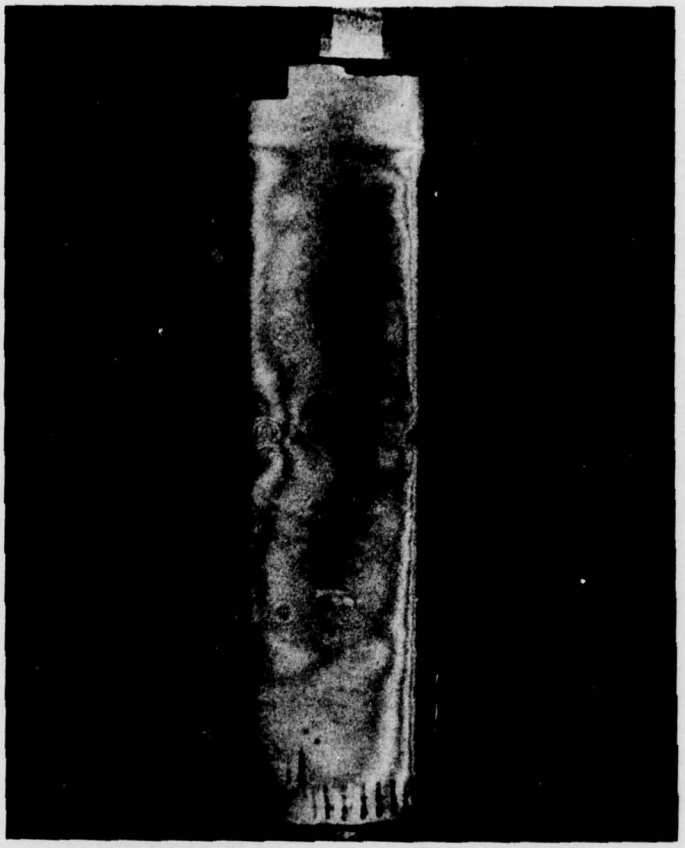

Horizontal Shear - Wedge Angle .25°

θ = 29.67°

λ = 6328 A

Δp = 20 psi

Figure 1-15. Circumferential Flaw - Filtered Image

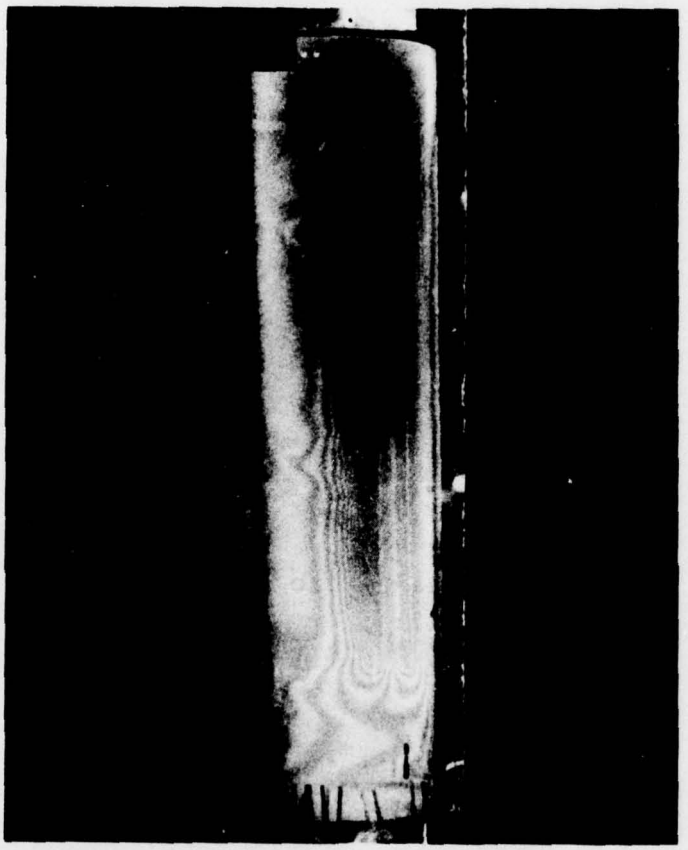

Horizontal Shear - Wedge Angle .25°

θ = 29.67°

λ = 6328 A

Δp = 20 psi

Figure 1-16. Longitudinal Flaw - Filtered Image

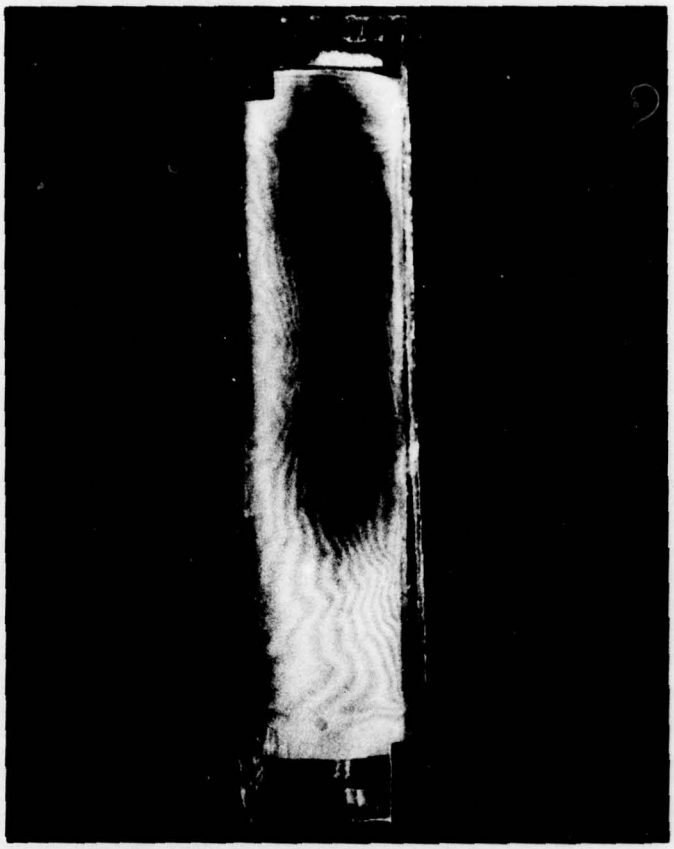

Horizontal Shear - Wedge Angle .25°

θ = 29.67°

λ = 6328 A

Δp = 20 psi

Figure 1-17. Spot Flaw - Filtered Image

PART II

DOUBLE EXPOSURE SPECKLE PHOTOGRAPHY

SINGLE BEAM ANALYSIS

An object is illuminated by a single beam as shown in Fig. 2.1.

The location of the light source is shown schematically as S. The point P is on the surface of the object.

Consider now a double exposure technique where the body is imaged two times on the same film before and after deformation.

For the first exposure the complex light amplitude can be expressed in the following form

$$\bar{E}(x_1,x_2) = \bar{A}(x_1,x_2) \exp[i\,\theta(x_1,x_2)] \tag{2.1}$$

where x_1 and x_2 are the film plane coordinates.

Suppose now the object is deformed and the point P is displaced to a point P'. Then the image on the film plane will be shifted to new coordinates x_1' and x_2'. Now the complex light amplitude is

$$\bar{E}'(x_1',x_2') = \bar{A}(x_1',x_2') \exp[i\,\theta(x_1',x_2') + \Delta\theta] \tag{2.2}$$

The intensity of the first exposure is

$$I_1 = \bar{E}_1 \bar{E}_1^*$$

or

$$I_1 = A^2(x_1,x_2) \tag{2.3}$$

The intensity of the second exposure is

$$I_2 = \bar{E}' (\bar{E}')^*$$

or

$$I_2 = A^2(x_1',x_2') \tag{2.4}$$

The total intensity is I_T where

$$I_T = I_1 + I_2 \tag{2.5}$$

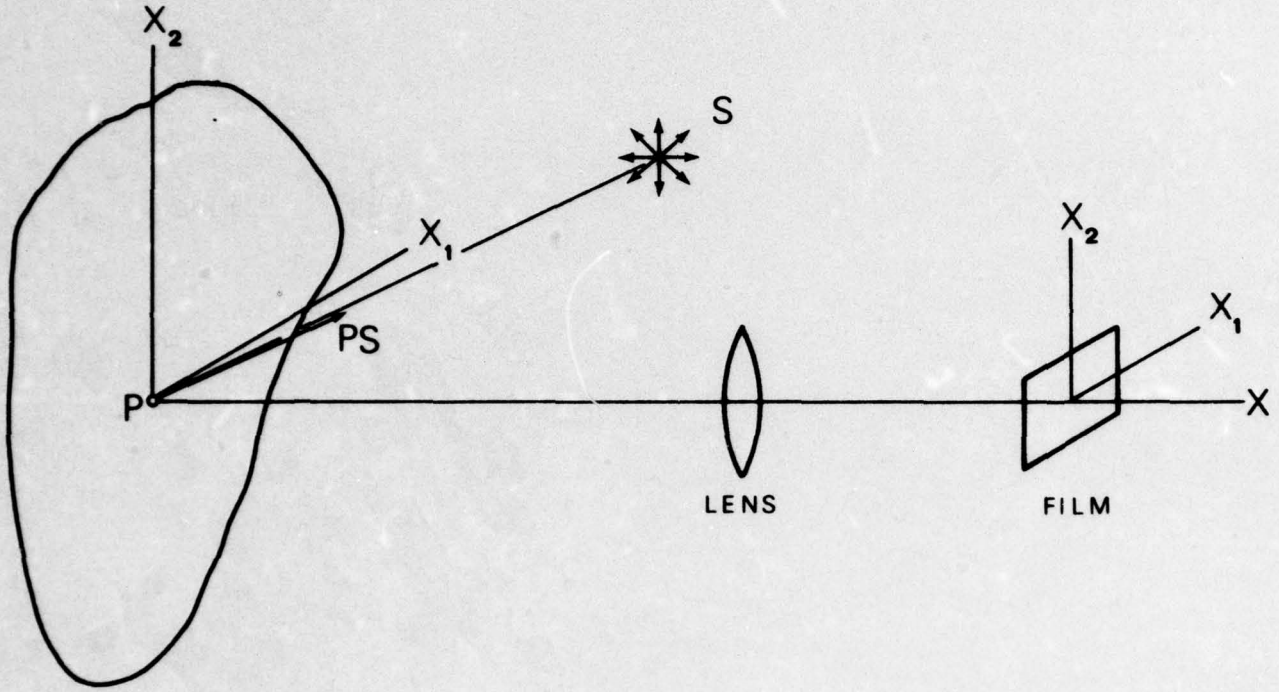

Figure 2.1 Arrangement for Single Beam Analysis

Physically what has been done is to image the point P at the location x_1, x_2 at the film plane coordinates. After the body has been deformed the point P now at P' is imaged at the film plane coordinates x_1', x_2'.

If the displacement vector $\vec{PP'}$ is written in the following manner

$$\vec{PP'} = u_i \bar{e}_i \tag{2.6}$$

Then the displacement vector in the film plane can be written as

$$[(\vec{PP'})\ x_1\ x_2] = M\ (\overline{PP'})\ x_1 x_2 \tag{2.7}$$
$$\text{FILM}$$

where M = magnification of camera, typically $M < 1$

and $u_{if} = M\ u_1$

$$u_{2f} = M\ u_2$$

The coordinates at the film plane for the second exposure are

$$x_1' = x_1 + u_{1f}$$

$$x_2' = x_2 + u_{2f}$$

and

$$(\vec{PP'})_f = u_{1f}\ \vec{e}_1 + u_{2f}\ \vec{e}_2 \tag{2.8}$$

The total intensity after the second exposure can be written in the form

$$I_T = A^2\ (x_1, x_2) + A^2\ (x_1 + u_{1f}, x_2 + u_{2f}) \tag{2.9}$$

Let the amplitude transmission of the photographic plate be $g(x,y)$. Let the amplitude of transmission be linear with exposure then (reasonable assumption for most films that are used)

$$g(x_1, x_2) = a + b\ I_T \tag{2.10}$$

where a,b are constants.

For convenience suppress the x_2 coordinate in the following discussion, thus

$$g(x) = a + b\ [A^2\ (x) + A^2\ (x + u_{1f})] \tag{2.11}$$

Burch and Tokarski* have derived the following expression

$$G(w) = \exp\left[\frac{izw^2}{2k}\right] \int g(x) \exp(-iwx)\, dx \qquad (2.12)$$

This expression is the Fourier Transform of the amplitude transmission function of the photographic plate where w is given by (Fig. 2-2)

$$w = \frac{2\pi}{\lambda} \tan\theta = \frac{2\pi x_s}{z\lambda} \qquad (2.13)$$

and x_s is the coordinate on the screen or Fourier Transform plane.

The equation for G(w) is derived from the Kirchoff diffraction formula and with eq (2.11)

$$G(w) = \exp\left[\frac{izw^2}{2k}\right] \int a+b\,[A^2(x) + A^2(x + u_{1f})] \exp(-iwx)dx \qquad (2.14)$$

let

$$\delta(w) = \int \exp(-iwx)dx \qquad (2.15)$$

where (w) is called the delta function

then

$$G(w) = a \exp\left[\frac{izw^2}{2k}\right] \delta(w) + b \exp\left[\frac{izw^2}{2k}\right] \int A^2(x) + A^2(x+u_{1f})] \exp[-iwx]\, dx \qquad (2.16)$$

Use the shift theorem on the second term

$$\int [A^2(x + u_{1f})] \exp[-iwx]\, dx = \int A^2(x) \exp(-iwx) \exp[iu_{1f}w]dx \qquad (2.17)$$

$$\text{Define } F[A] = \int A^2(x) \exp(-iwx)dx \qquad (2.18)$$

Thus,

$$G(w) = a \exp\left[\frac{izw^2}{2k}\right] \delta(w) + b \exp\left[\frac{izw^2}{2k}\right] F[A]\,[1 + \exp(iwu_{1f})] \qquad (2.19)$$

---

* Burch, J. M. and Tokarski, J. M. J. "Production of Multiple Beam Fringes from Photographic Scatterers" 1968 Optica Acta, 15, pp. 101-111.

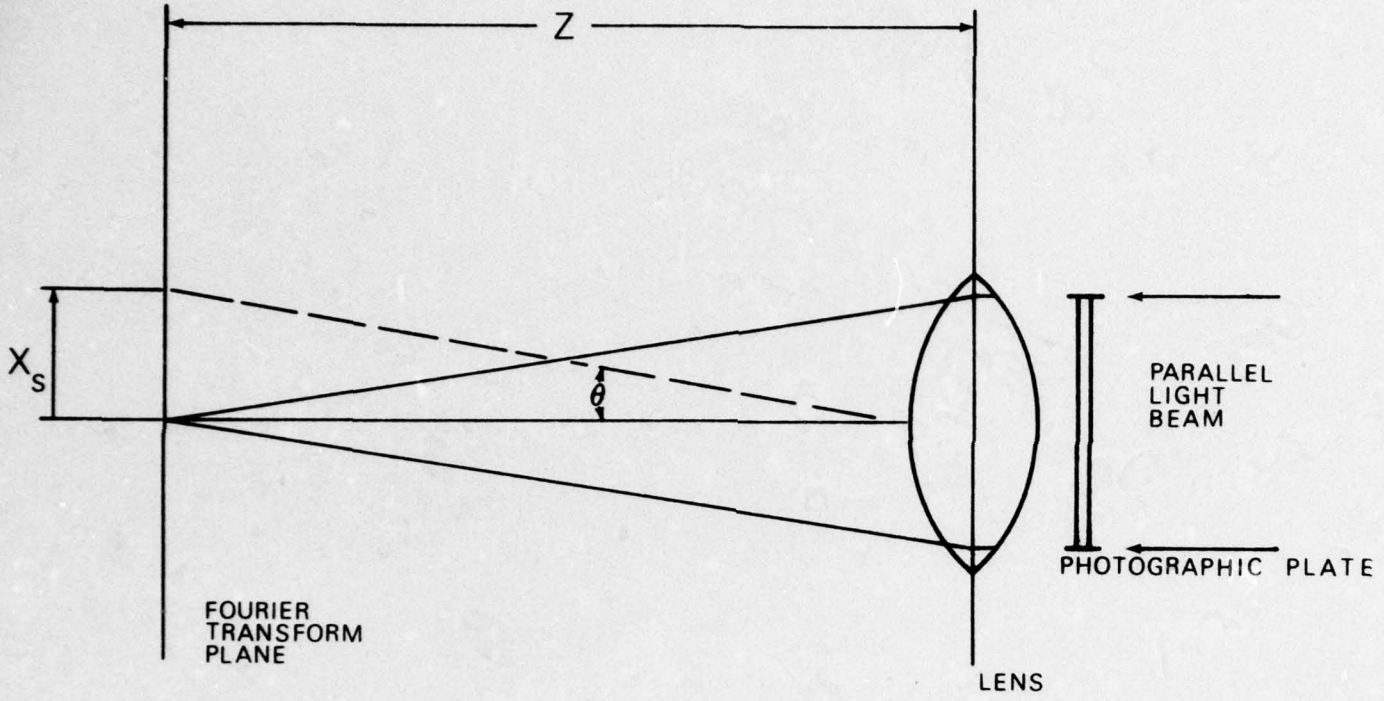

Figure 2.2 Arrangement for Transform Analysis

The intensity at the transform plane is

$$I_F = G(w)\, G(w^*) \tag{2.20}$$

or

$$I_F = b^2 F[A]^2 [\, 1 + \exp[-iwu_{1f}] + \exp[\, iwu_{1f}] \,]$$

or

$$I_F = 2b^2 F[A]^2 [1 + \cos(wu_{1f})] \tag{2.21}$$

A fringe will be defined when $I_F = 0$

therefore

$$[1 + \cos(wu_{1f})] = 0$$

when

$$\cos(wu_{1f}) = -1$$

or

$$w\, u_{1f} = (2n-1)\pi$$

Recall that $w = \frac{2\pi}{\lambda}\left(\frac{x_s}{z}\right)$

and

$$n = \left(\frac{x_s}{\lambda z}\right) u_{1f} + \frac{1}{2} \tag{2.22}$$

Now to interpret Eq (2.22) reference Fig. 2-3. The information at location x_s is selected by placing an aperture to pass only the light in the immediate neighbor of x_s. This light is then imaged on film. Thus x_s being fixed the imaged fringe information is proportional to u_{1f} or

$$u_{1f} = (n - \tfrac{1}{2})\, \frac{\lambda z}{x_s}\, m_1 \tag{2.23}$$

where m_1 is the magnification of the new image relative to the original object. An experiment was set up to note the results of the theory reflected in eq. (2.23). The experimental arrangement is shown in Fig. 2-4. The coordinates relative to the cantilever beam are shown in Fig. 2-5. Other data include

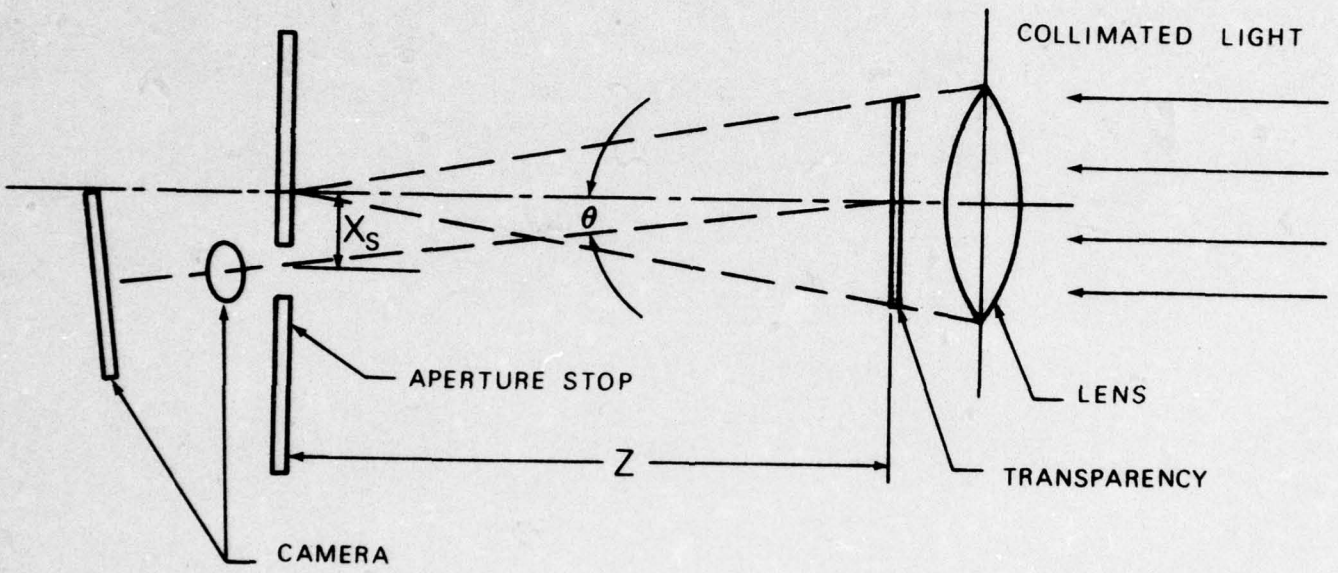

Figure 2.3 Arrangement for Data Collection

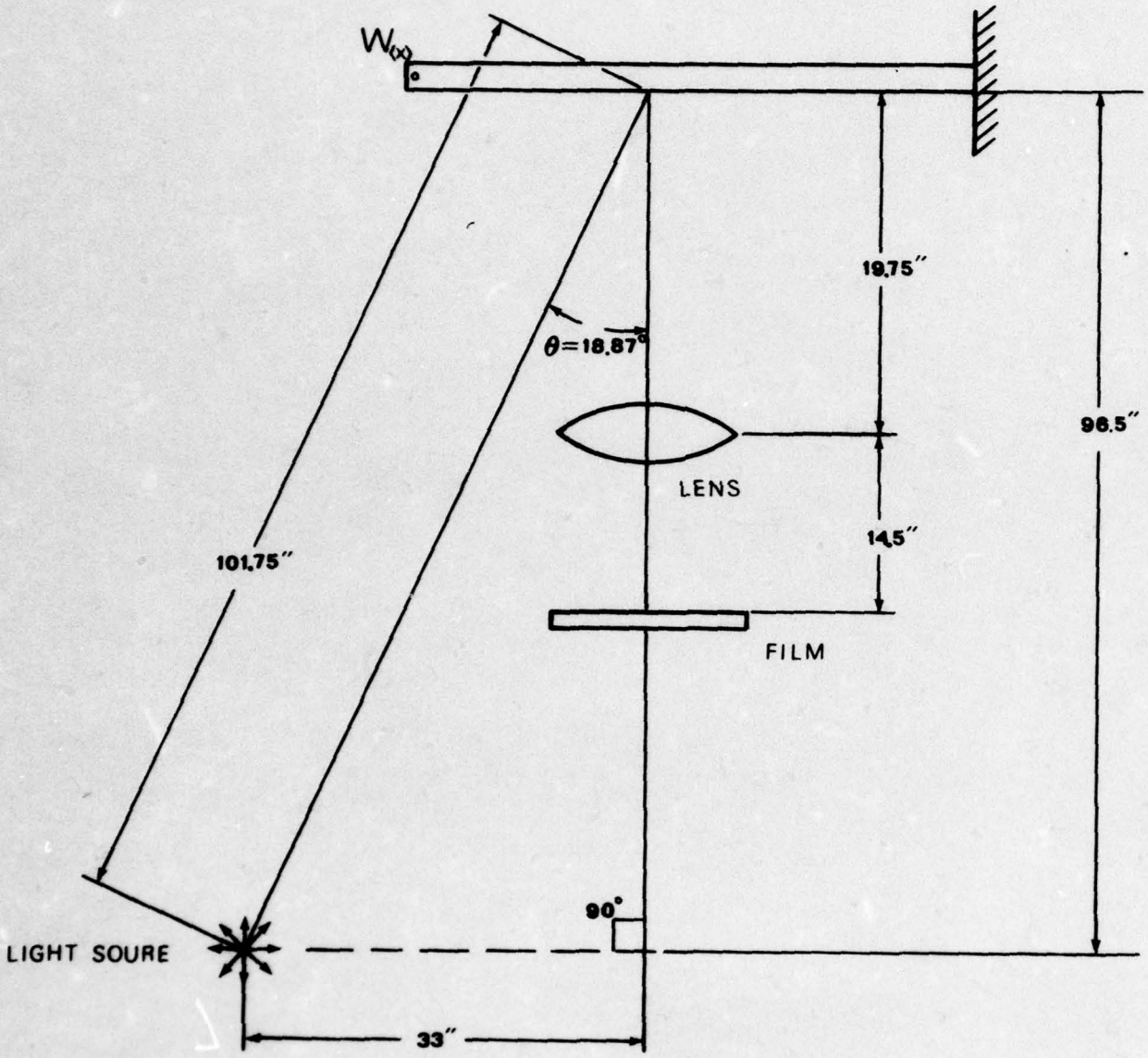

Figure 2.4 Experimental Set Up

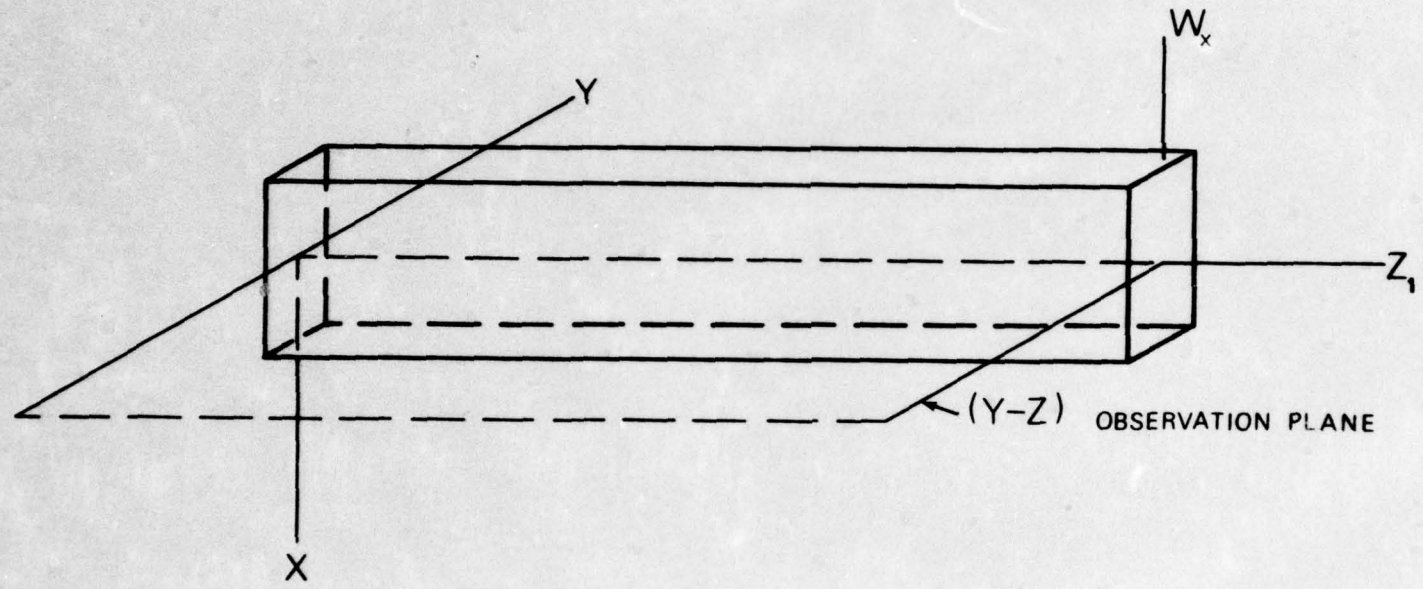

Figure 2.5 Cantilever Beam

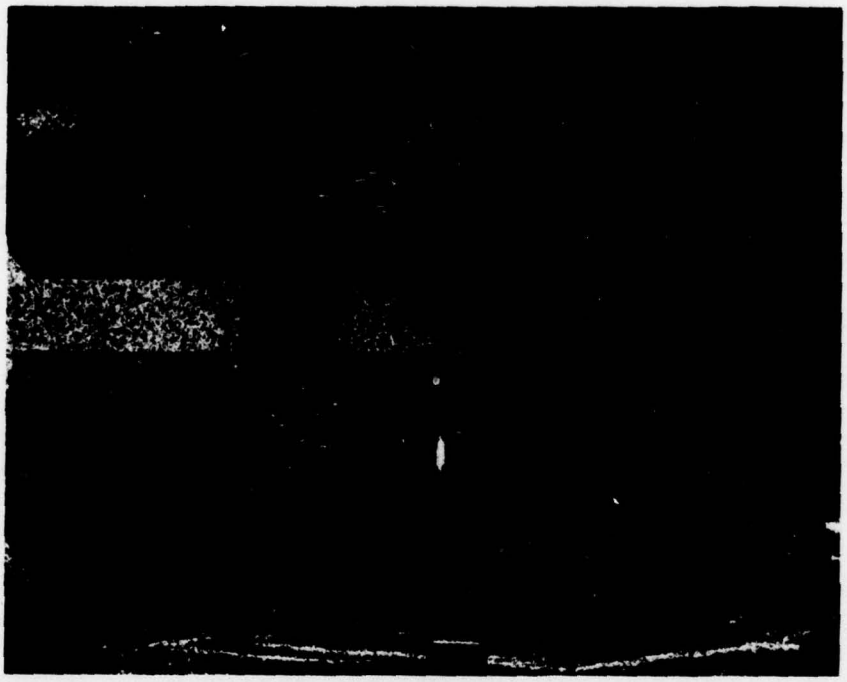

Fig. 2-6. CANTILEVER BEAM - YOUNGS FRINGES

$\theta = 18.87^{o}$

$\lambda = 5145A$

$\delta = .003"$

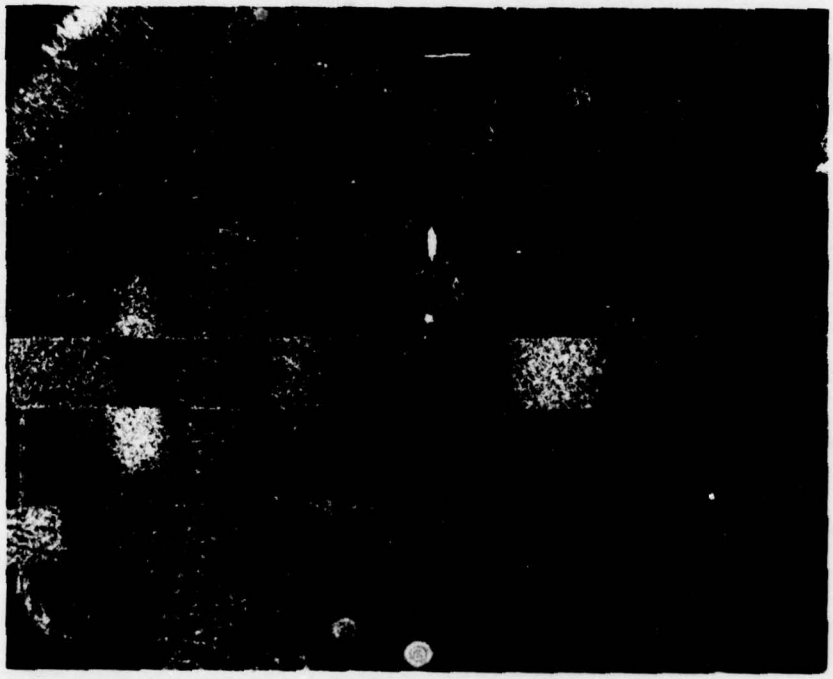

Fig. 2-7. CANTILEVER BEAM - YOUNGS FRINGES

$\theta = 18.87^{o}$

$\lambda = 5145A$

$\delta = .006"$

z_1 = coordinate location on model surface

z = 33 inches

x_s = 0.98 inch

λ = 20.26 microinches

ν = 0.37

Scale factor = 4.55 inches = model dimension/photograph dimension

Deflection on end of cantilever beam equaled 0.003 inch and 0.006 inch (in a direction parallel to film plane) cantilever beam dimensions were 6" length, 0.250 inch thickness, and 0.500 inch height.

Experimental results are pictured in Fig. 2-6,7. For comparison with theory let

u_x = displacement in the x - direction

u_y = displacement in the y - direction

u_{z1} = displacement in the z_1 - direction

and for the cantilevel beam examined

$$u_{z1} >> u_x$$

therefore

$$n = \frac{x_s}{\lambda z} \frac{M3\delta}{1^3} \left[\frac{\nu}{2} (1-z_1) (x^2-y^2) - \frac{1}{6} z_1^3 + \frac{1}{2} z_1^2 1 \right] + \frac{1}{2} \qquad (2.24)$$

where the displacement u_z was given by eq 1.22. A comparison is shown in Fig. 2-8. The agreement is "good". Locating flaws in composite structures by this technique is difficult because of the indistinct (relative to holography) fringes, but is a full field technique.

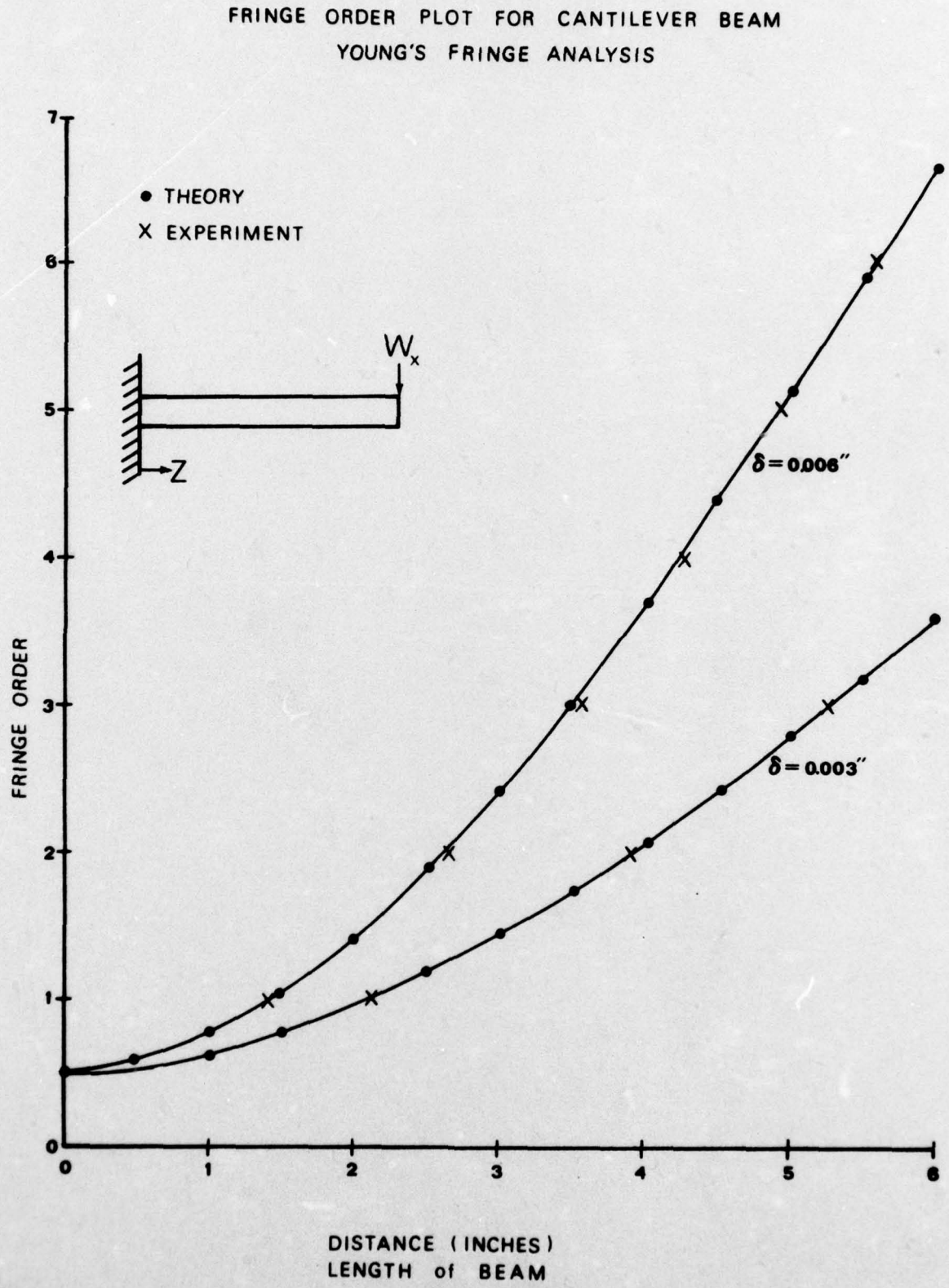

Figure 2.8 Comparison of Theory and Experiment

PART III

SPECKLE INTERFEROMETIC ANALYSIS USING YOUNG'S FRINGES

Theory for this technique as applied to flaw detection is included in Technical Report RL-76-18, "Quantification of Flaws in Fibered Composite Structures Using Interferometric Fringe Patterns" by Mullinix, Ranson, Swinson, Cost, U. S. Army Missile Command, Redstone Arsenal, Alabama 35809, April 1976.

Maxima occur when

$$u = m_1 \frac{\lambda f}{\underline{X}} \quad \text{for } m_1 = 1, 2, 3, - - - \tag{3.1}$$

where

u = in plane displacement at a point between loaded and unloaded model

λ = wave length of light used in data analysis

f = distance from film record to screen

$\underline{X}$ = fringe spacing as noted on screen

m_1 = fringe order

Reference Fig. 3-1 and 3-2 for arrangement of data collection and data analysis. The experimental arrangement is seen in Fig. 3-3. The models were loaded by pressurizing the vessels to 120 psi. The double exposed film was analyzed by taking data at 0.1 inch intervals (Fig. 3-4), the x,y axis was located arbitrarily. Fig. 3-5 shows the effect on the fringes in the vicinity of a flaw. At each location (x,y) the fringe spacing was measured in the "y" direction (axis of the cylinder) and displacement in the y direction calculated using eq. (3-1). The results of the spot flaw illustrated in Fig. 3-6 are shown in Fig. 3-7 thru 12. The results of the longitudinal flaw illustrated in Fig. 3-13 are shown in Figs. 3-14 thru 19. The results of the circumferential flaw illustrated

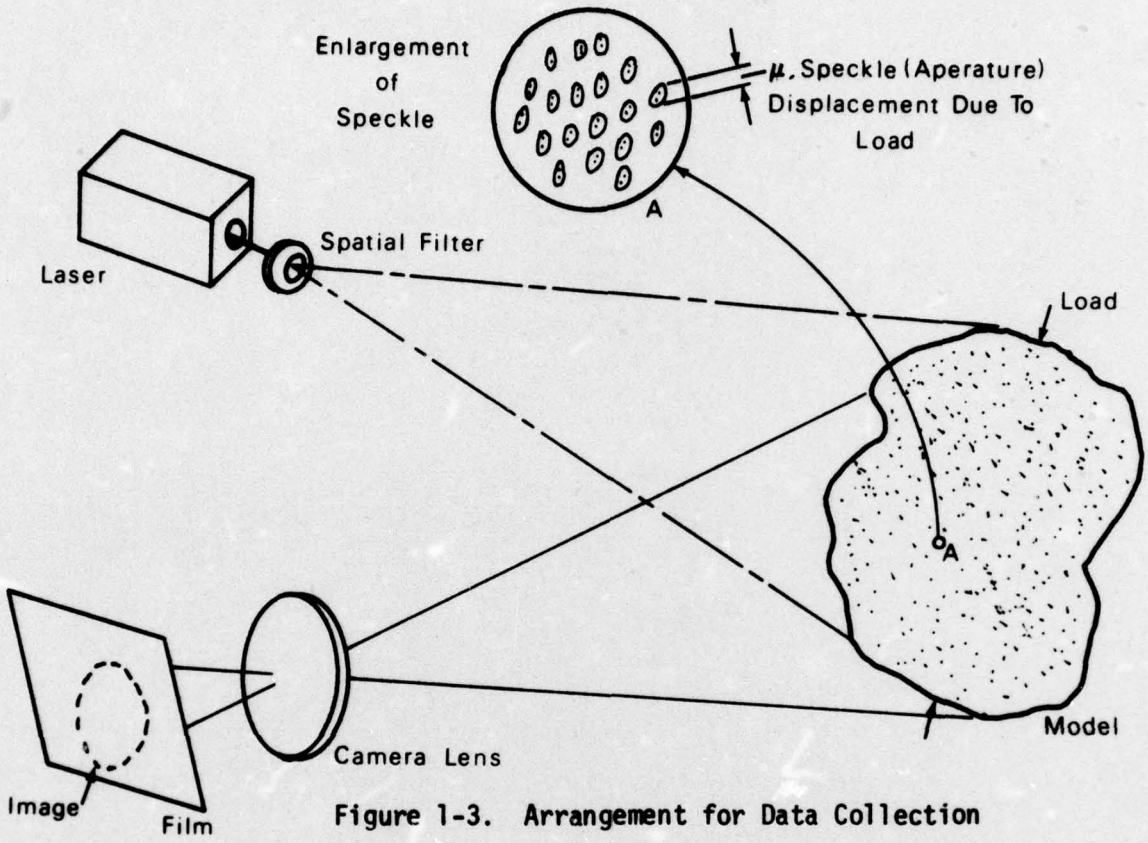

Figure 1-3. Arrangement for Data Collection

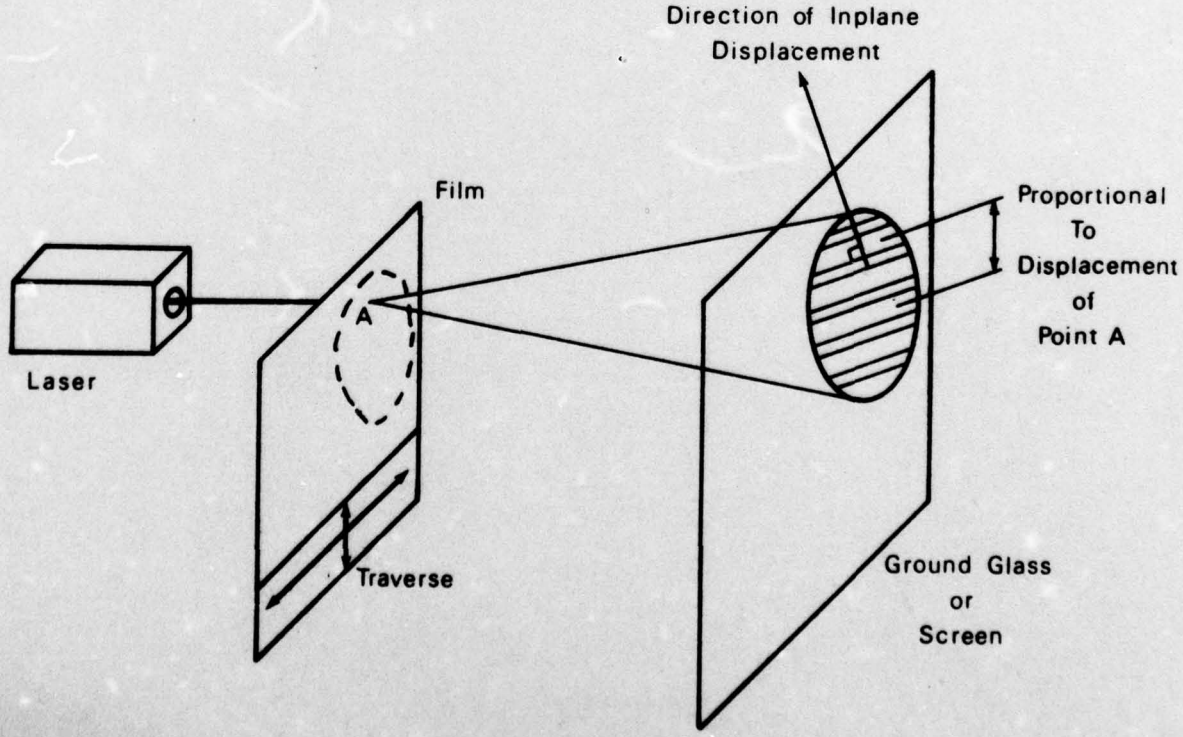

Figure 3-2. Analysis of Film

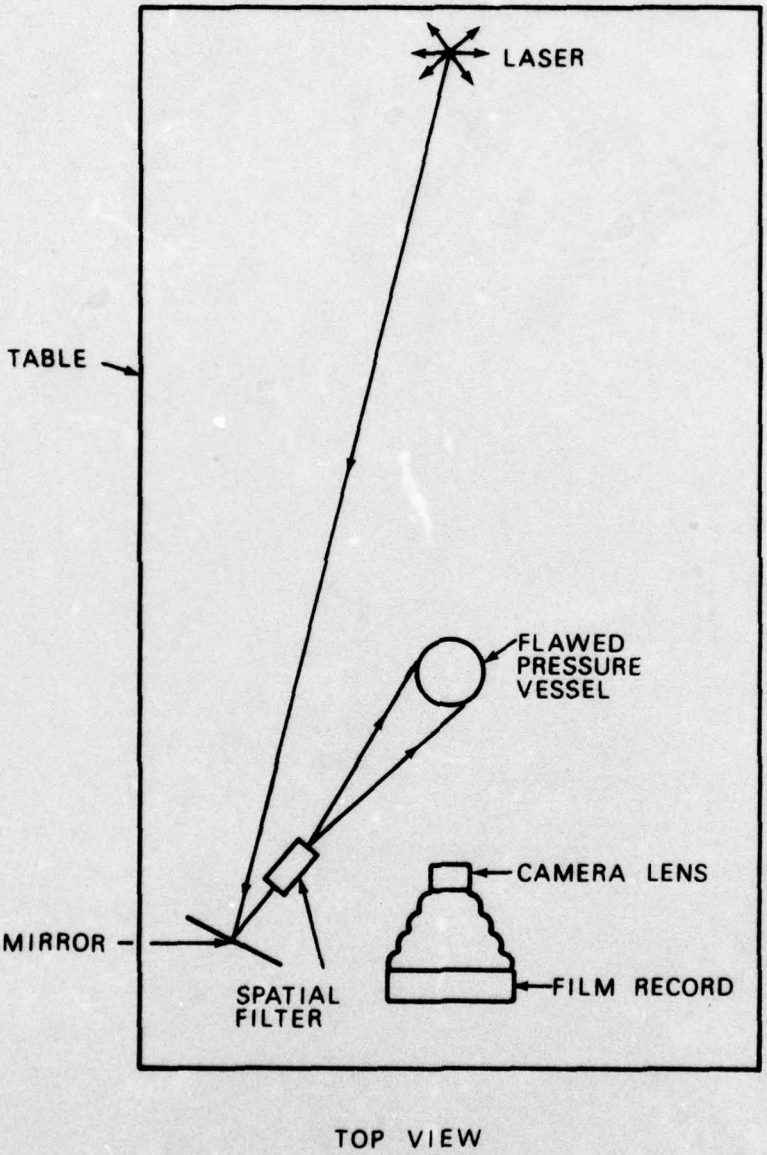

Figure 3-3. Experimental Arrangement

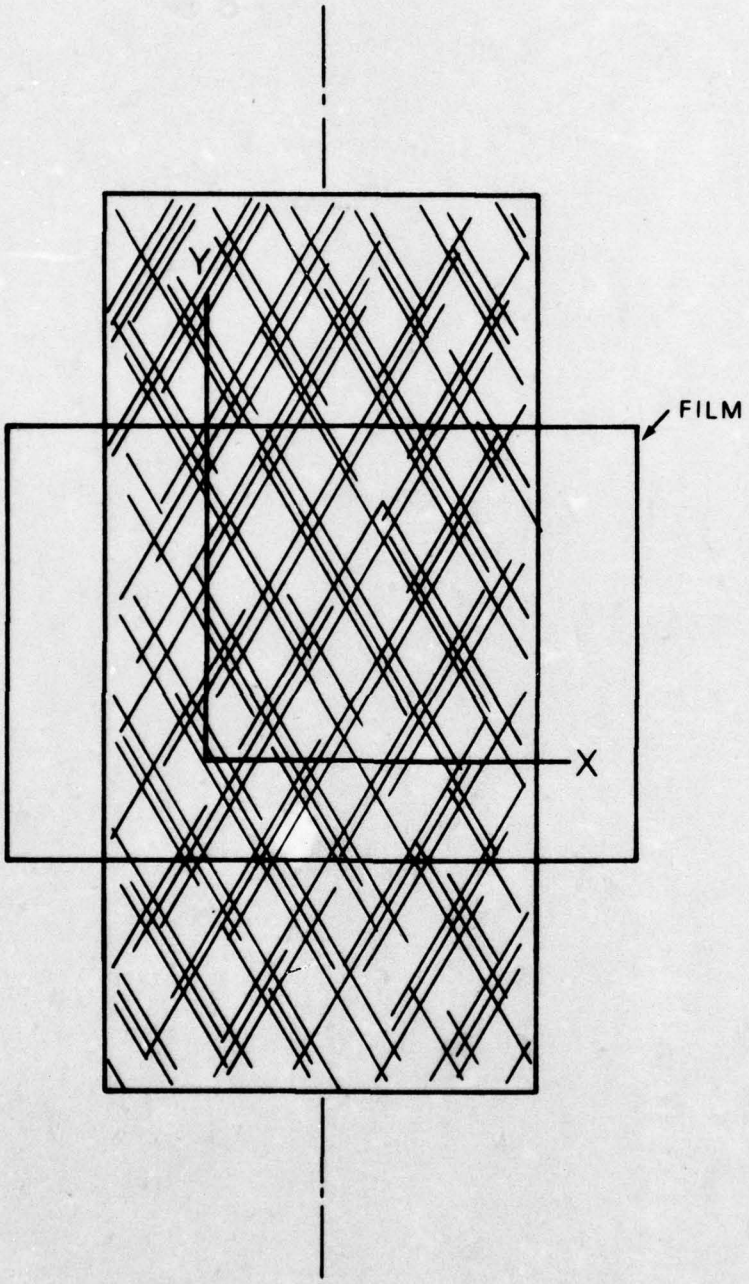

Figure 3-4. Coordinate Axis

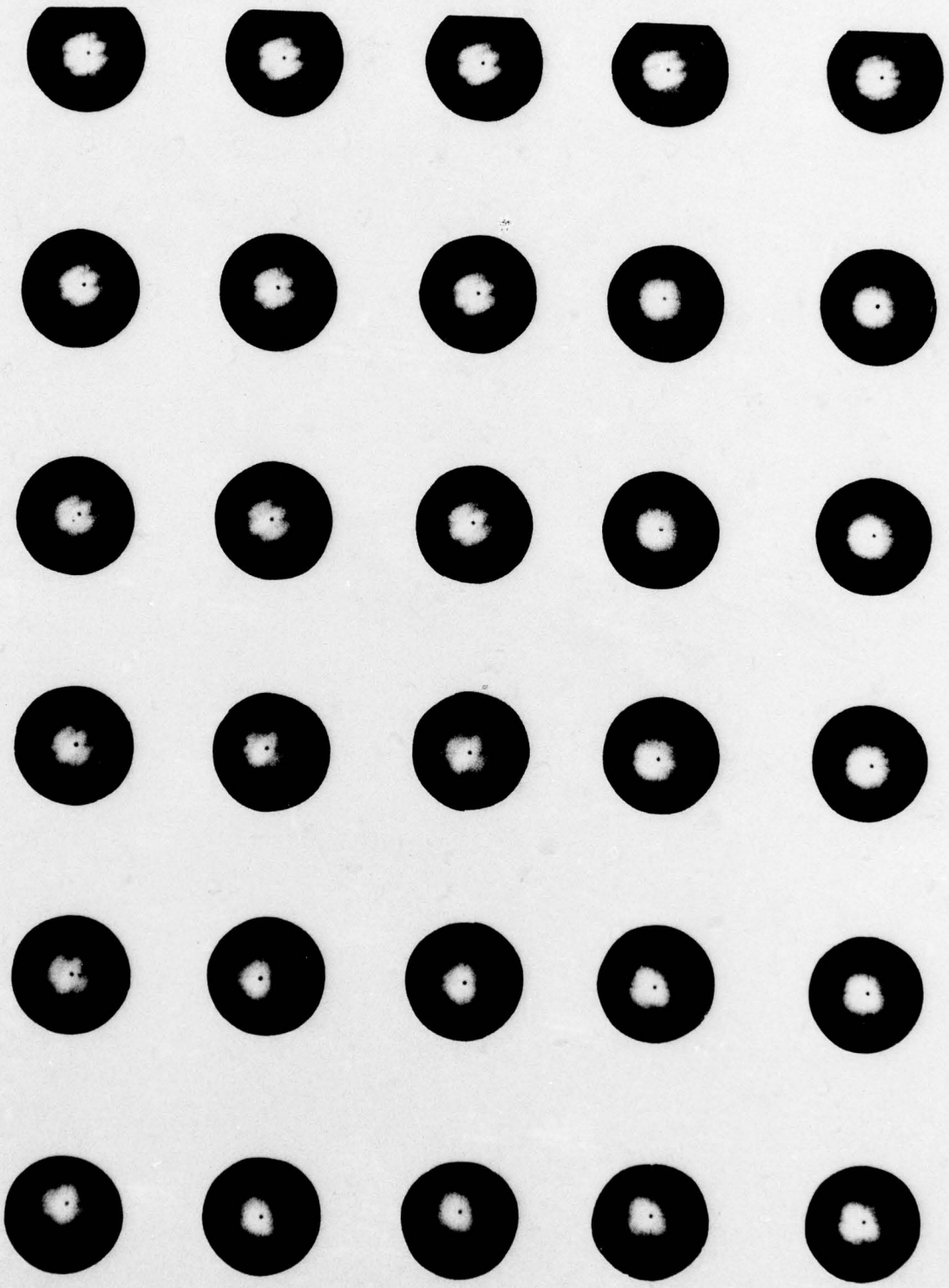

Figure 3-5. Fringe Pictures (Every 0.2 in)

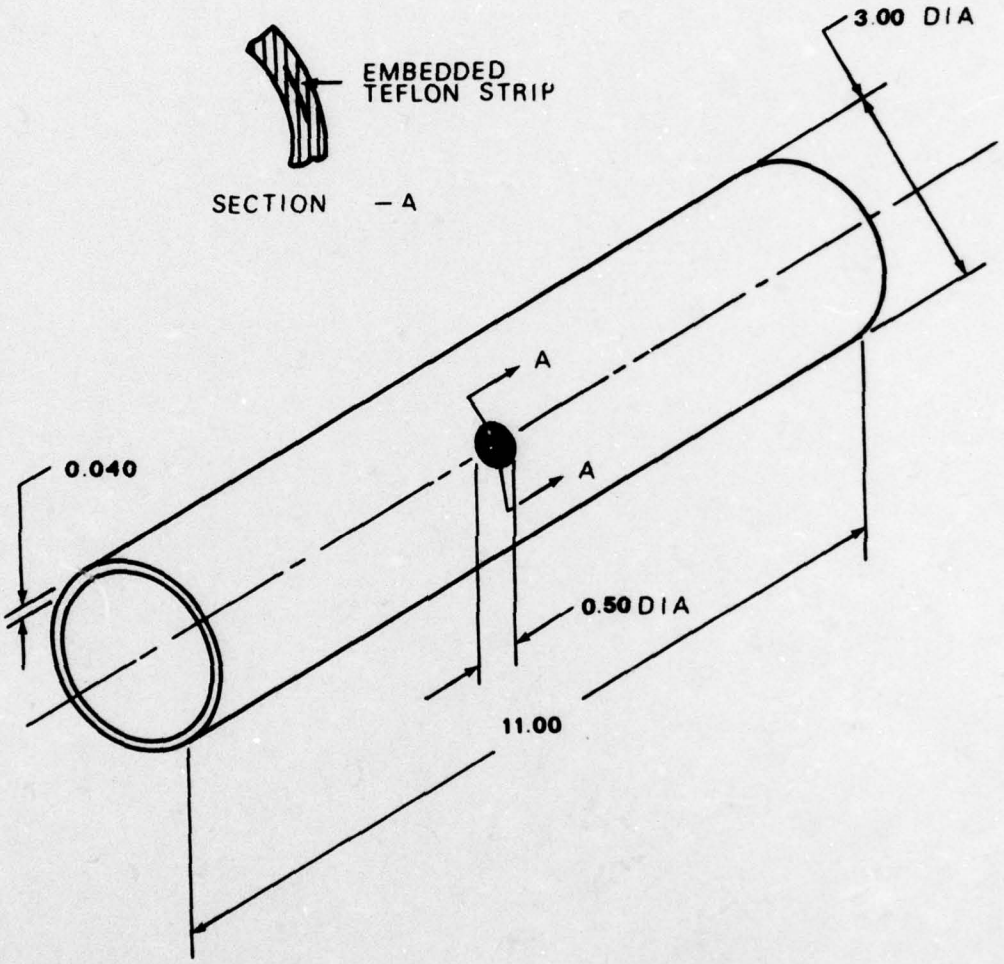

Figure 3-6. Spot Flaw

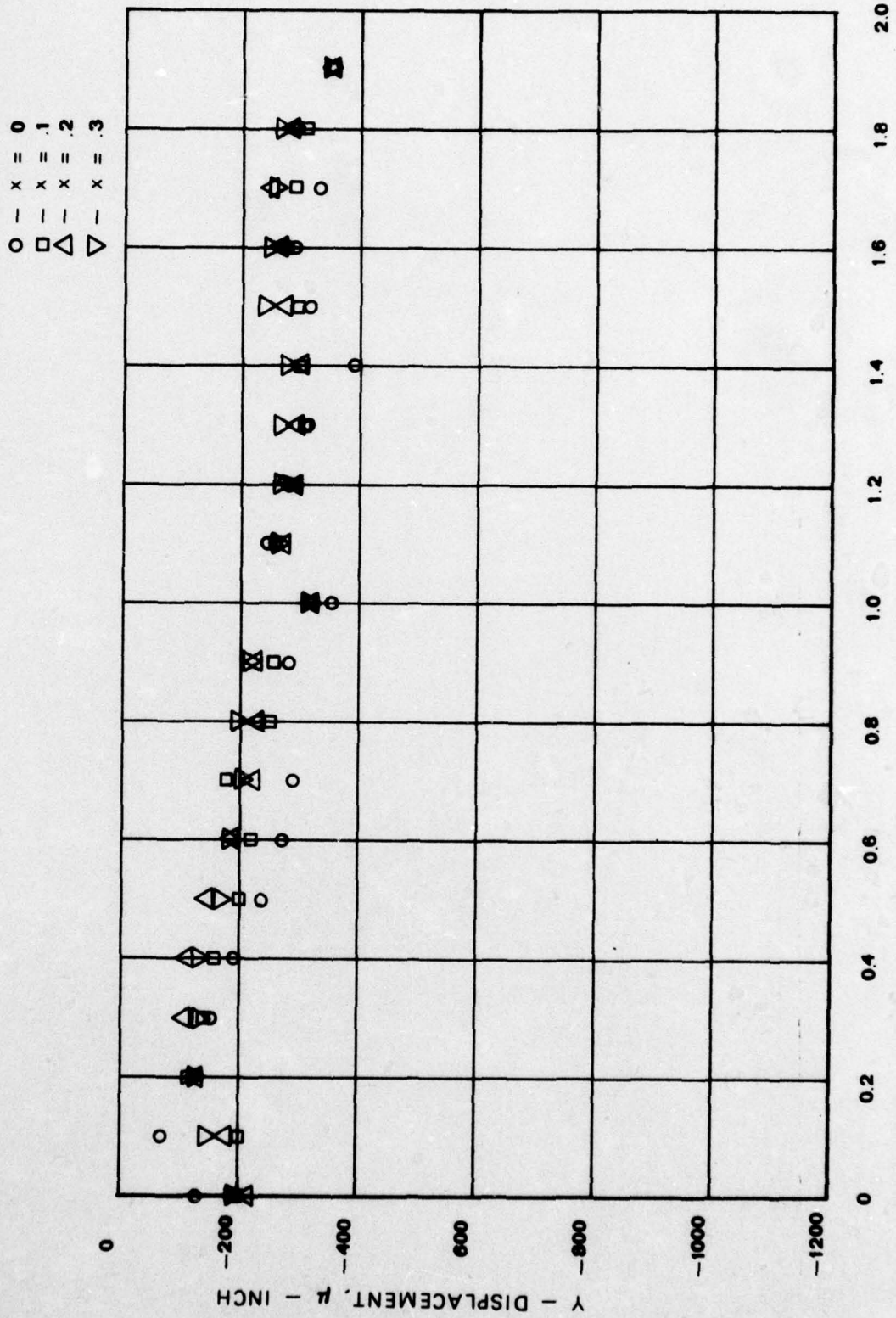

Figure 3-7. y-Displacement as a Function of y-Coordinate for the Spot Flaw Cylinder (x=0.0 - x=0.3)

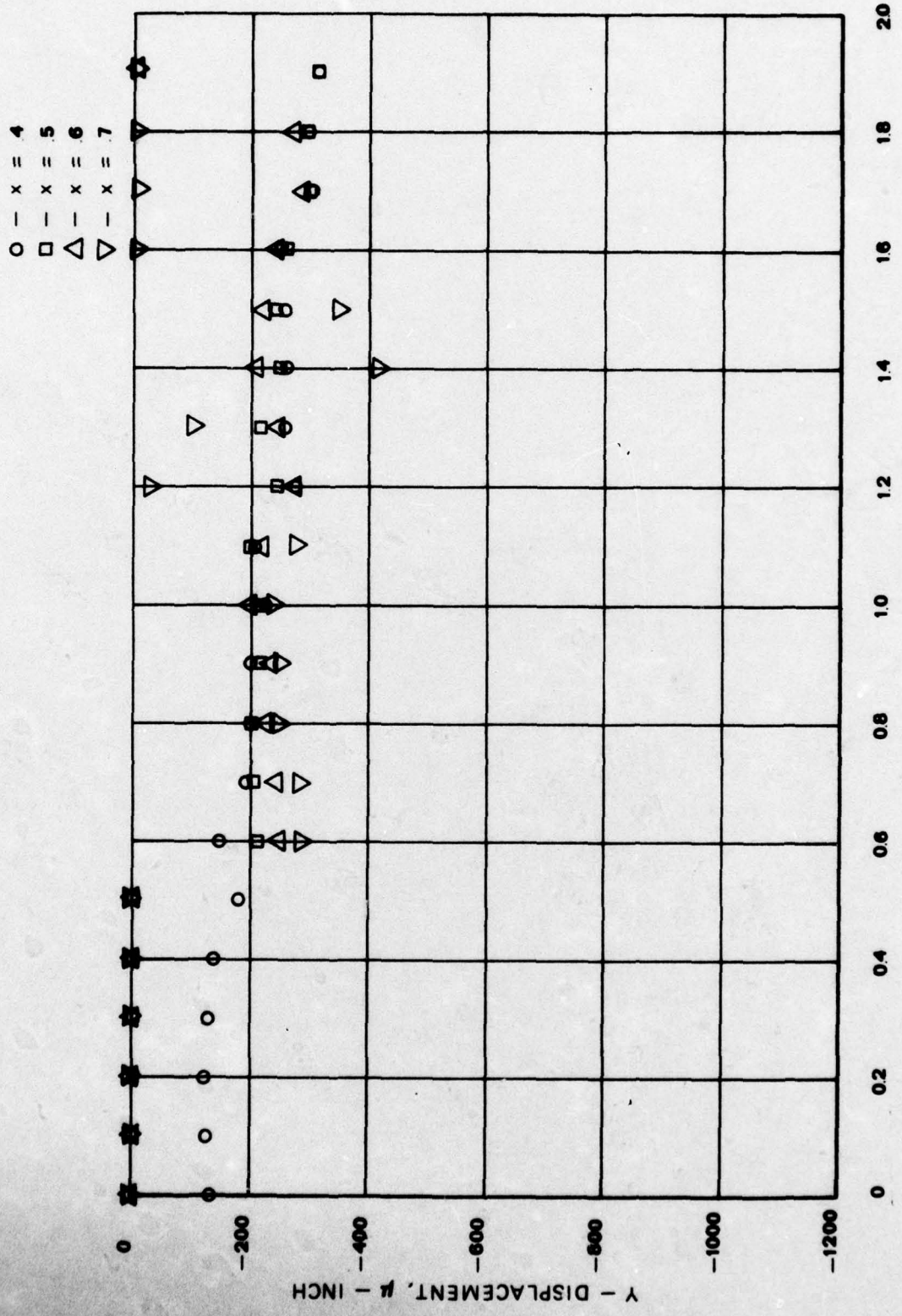

Figure 3-8. y-Displacement as a Function of y-Coordinate for the Spot Flaw Cylinder (x=0.4 - x=0.7)

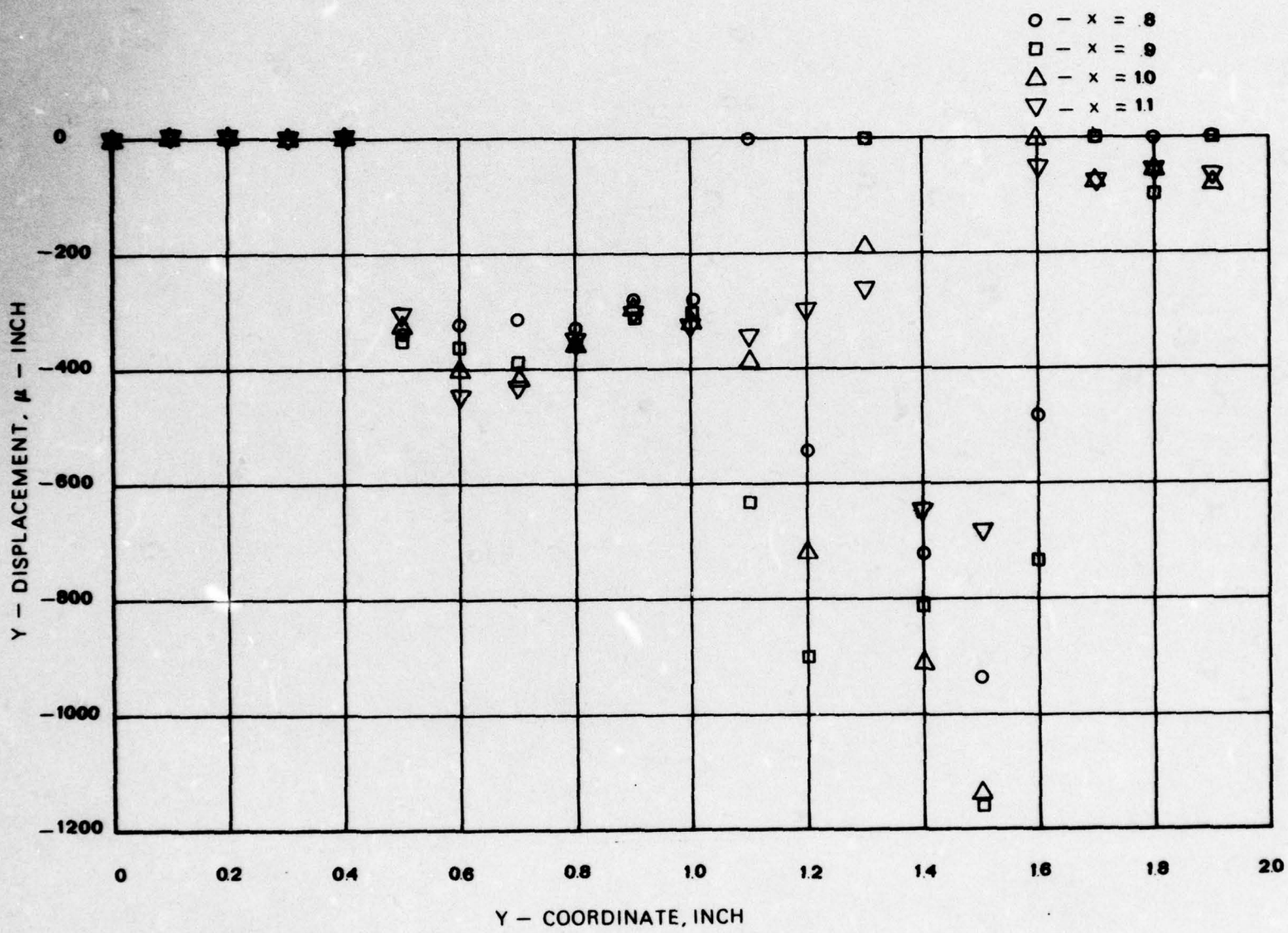

Figure 3-9. y-Displacement as a Function of y-Coordinate for the Spot Flaw Cylinder (x=0.8 - x-1.1)

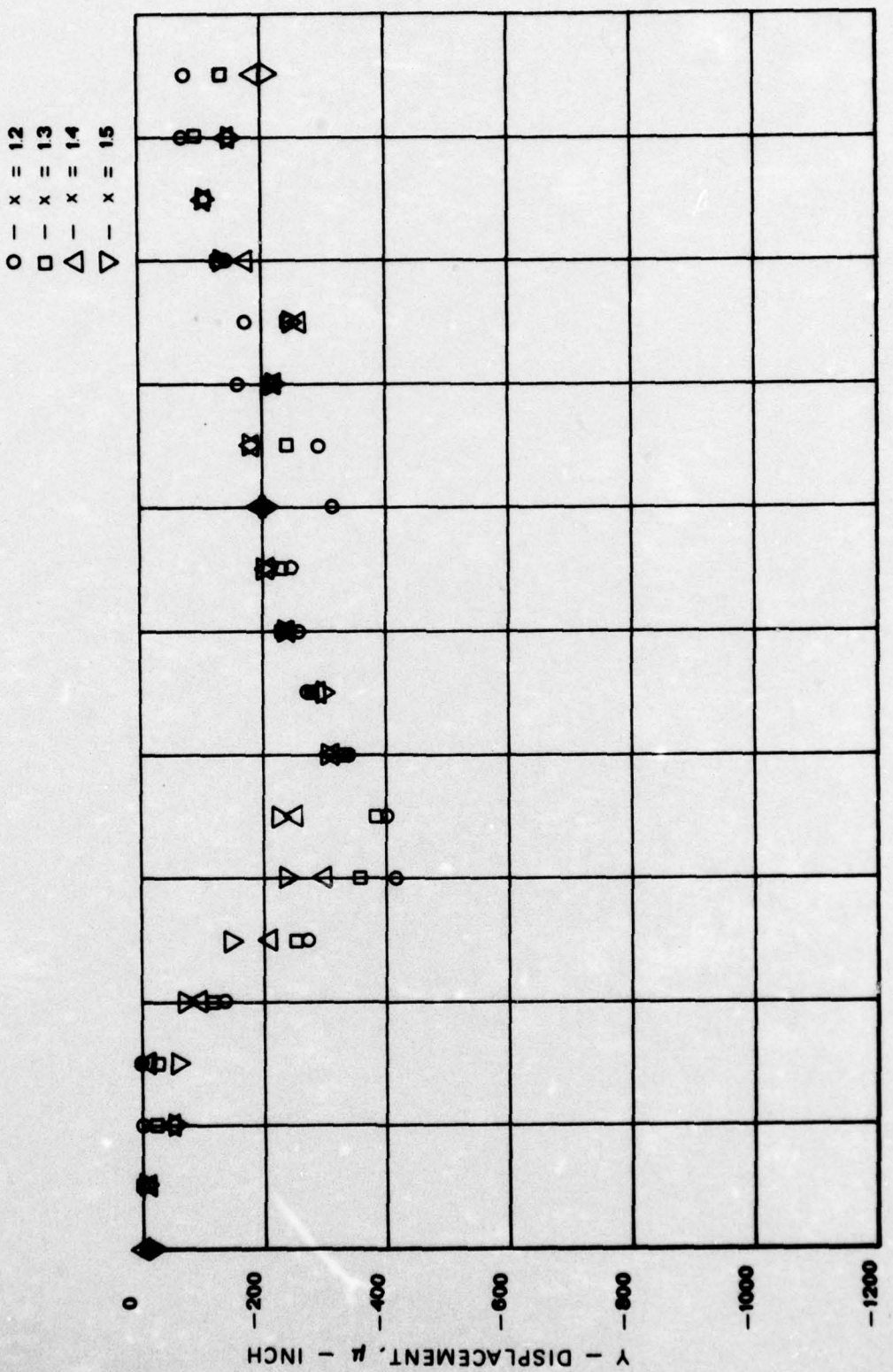

Figure 3-10. y-Displacement as a Function of y-Coordinate for the Spot Flaw Cylinder (x=1.2 - x=1.5)

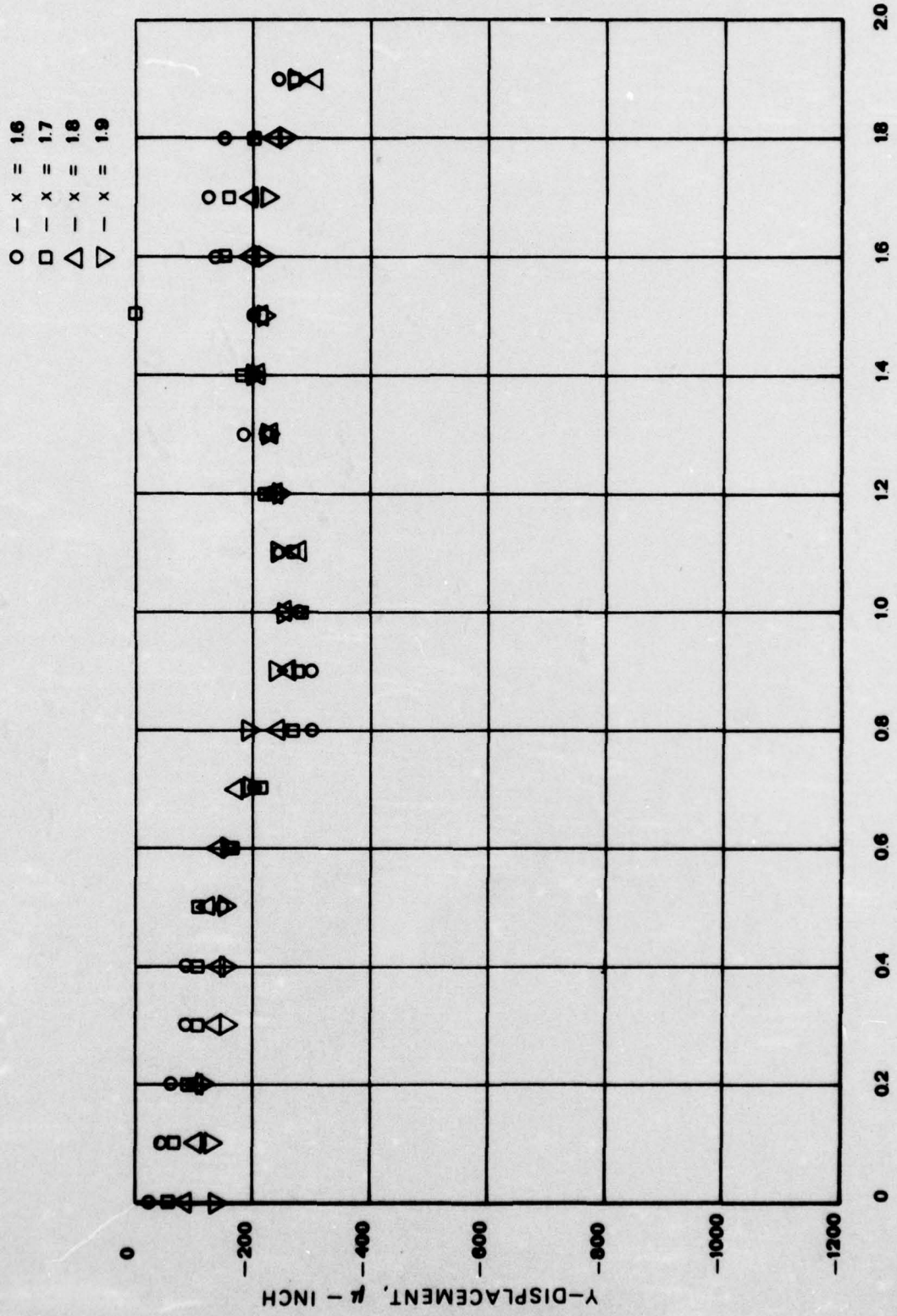

Figure 3-11. y-Displacement as a Function of y-Coordinate for the Spot Flaw Cylinder (x=1.6 - x=1.9)

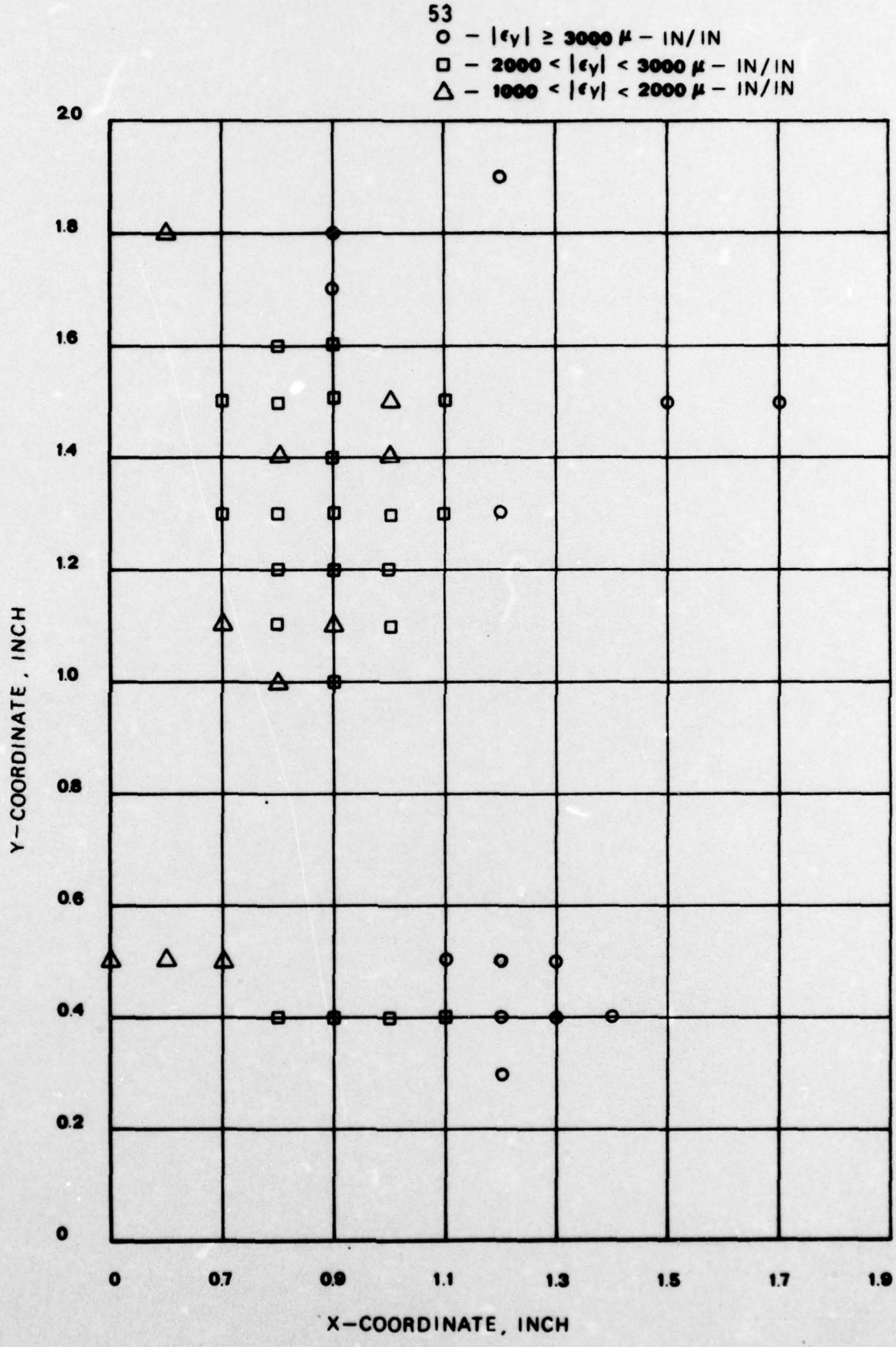

Figure 3-12. Strain Distribution for Spot Flaw Cylinder

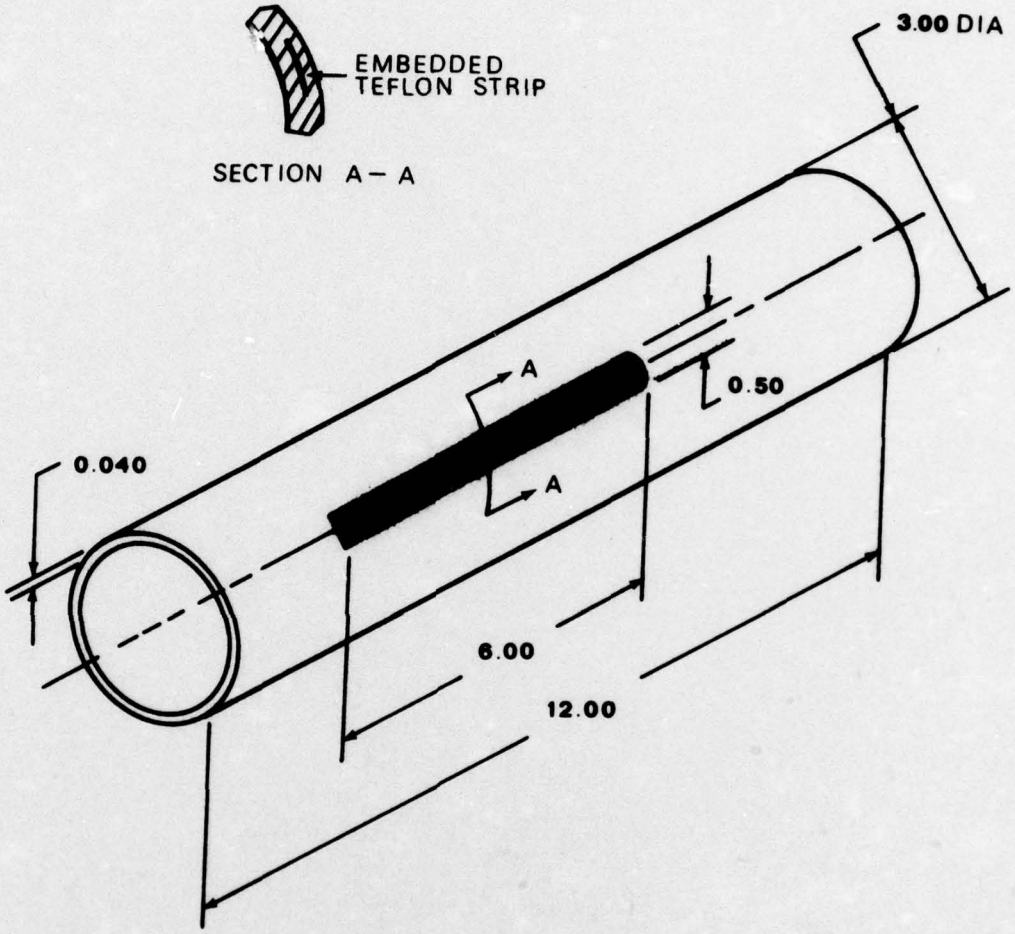

Figure 3-13. Longitudinal Flaw

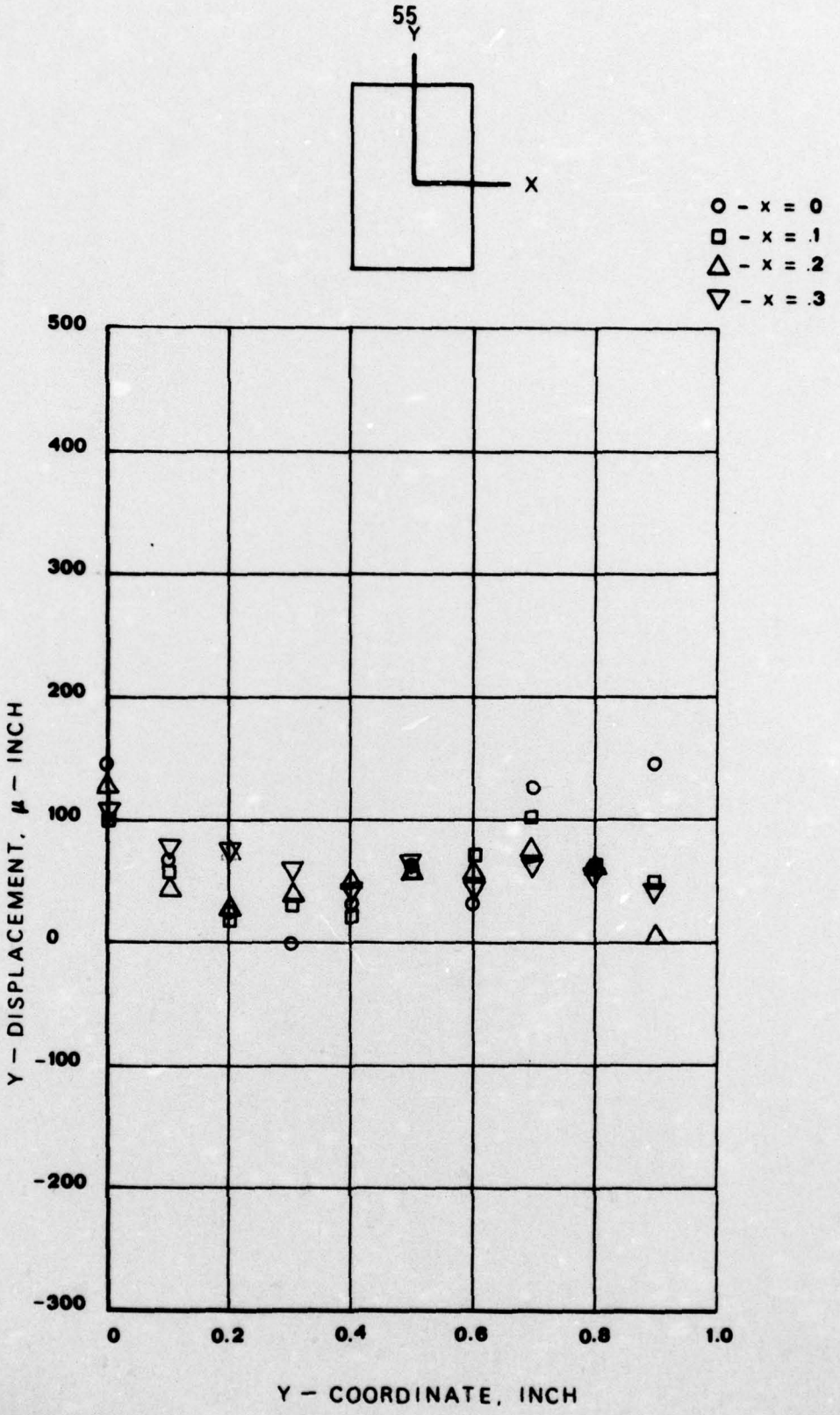

Figure 3-14. y-Displacement as a Function of y-Coordinate for Longitudinal Flaw (x=0 - x=0.3)

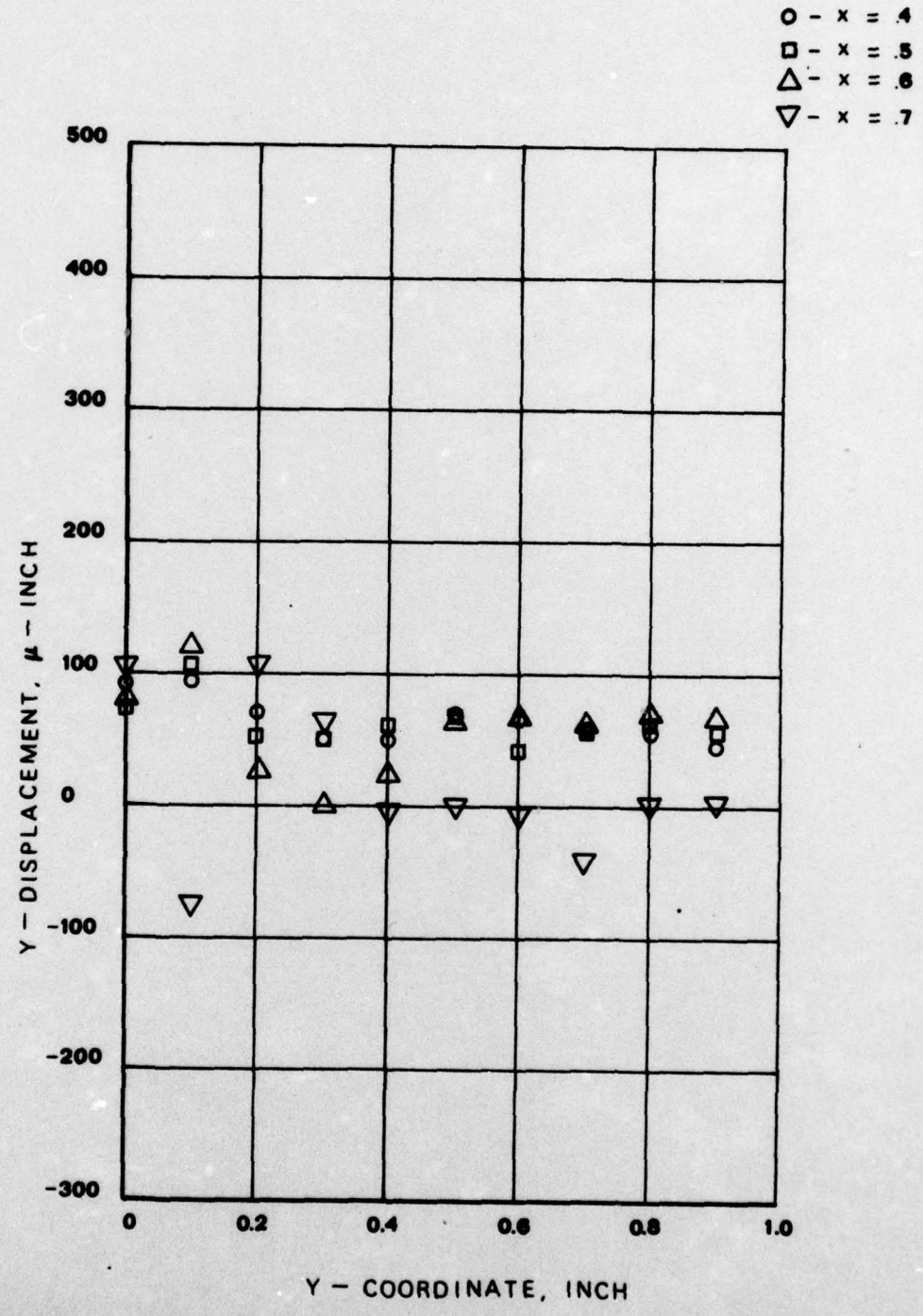

Figure 3-15. y-Displacement as a Function of y-Coordinate for Longitudinal Flaw (x=0.4 - x=0.7)

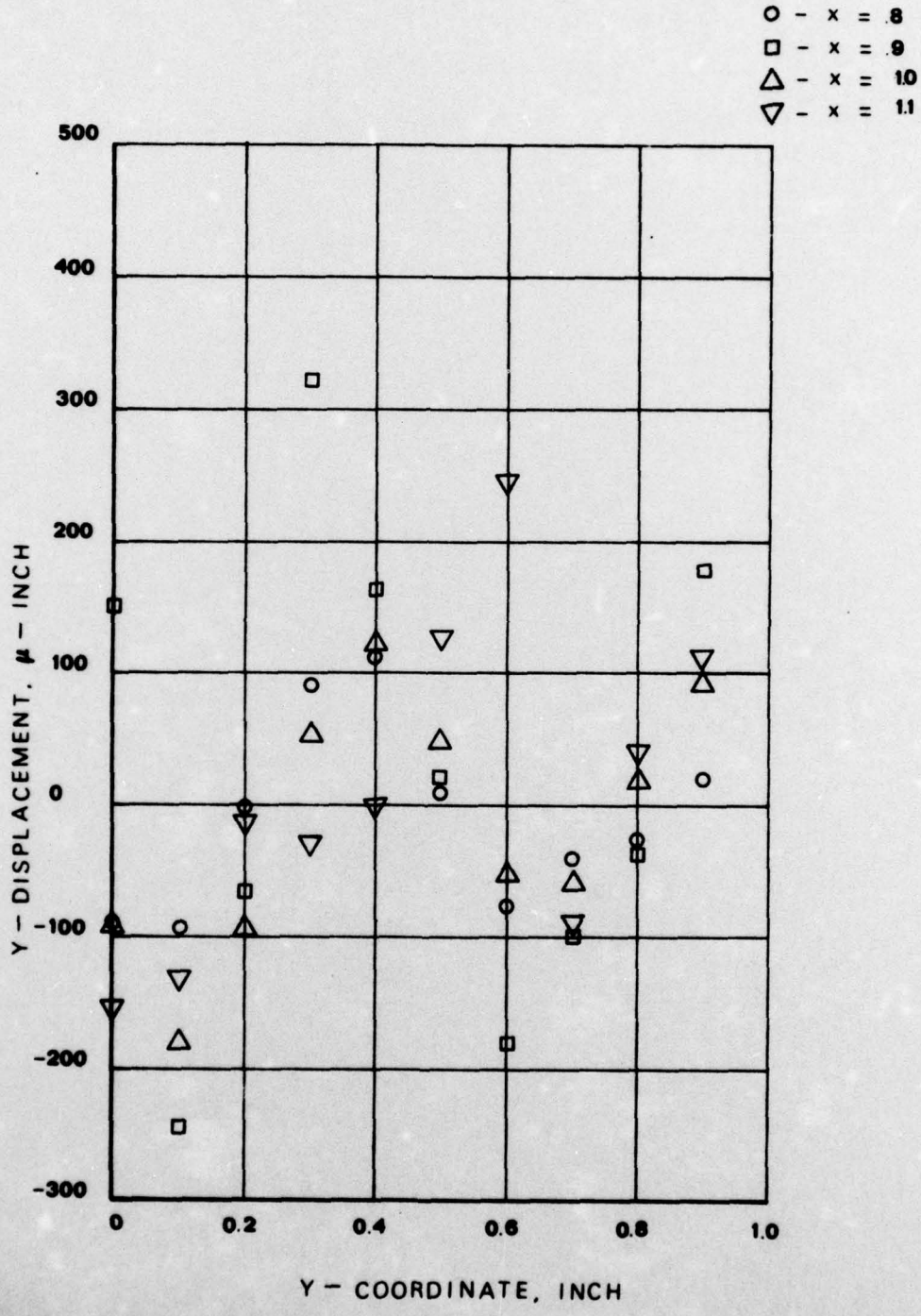

Figure 3-16. y-Displacement as a Function of y-Coordinate for Longitudinal Flaw (x=0.8 - x=1.1)

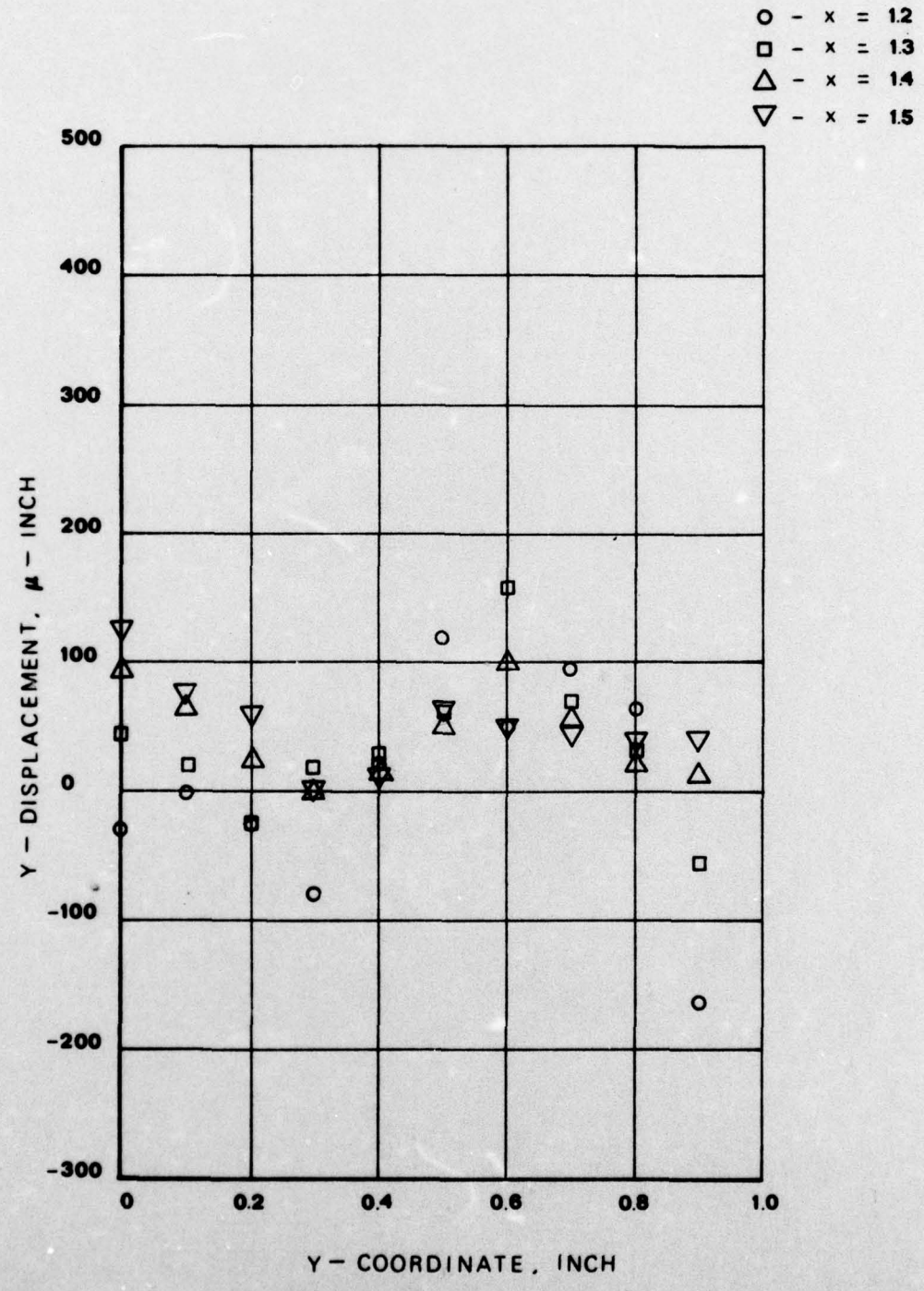

Figure 3-17. y-Displacement as a Function of y-Coordinate for Longitudinal Flaw (x=1.2 - x=1.5)

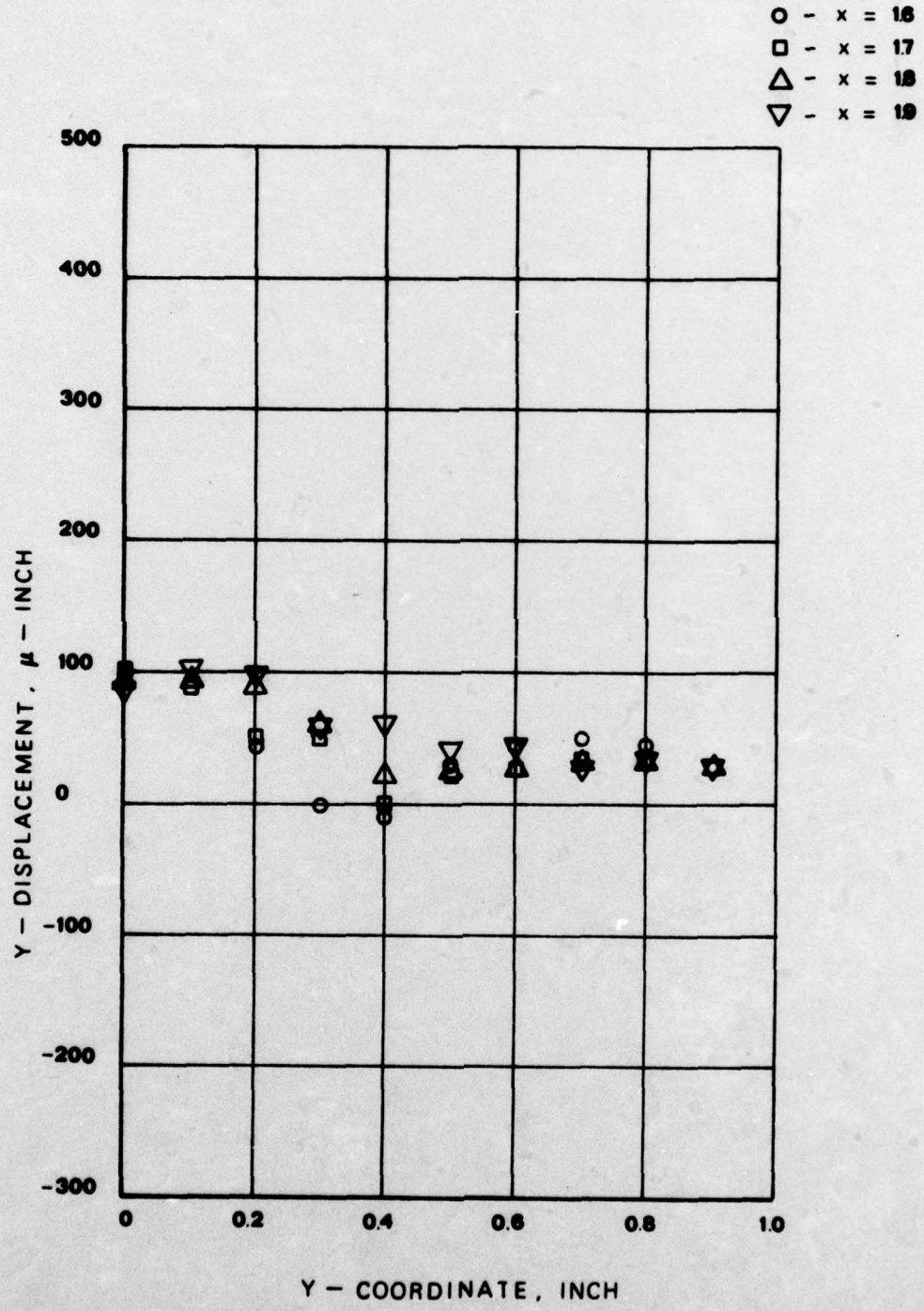

Figure 3-18. y-Displacement as a Function of y-Coordinate for Longitudinal Flaw (x=1.6 - x=1.9)

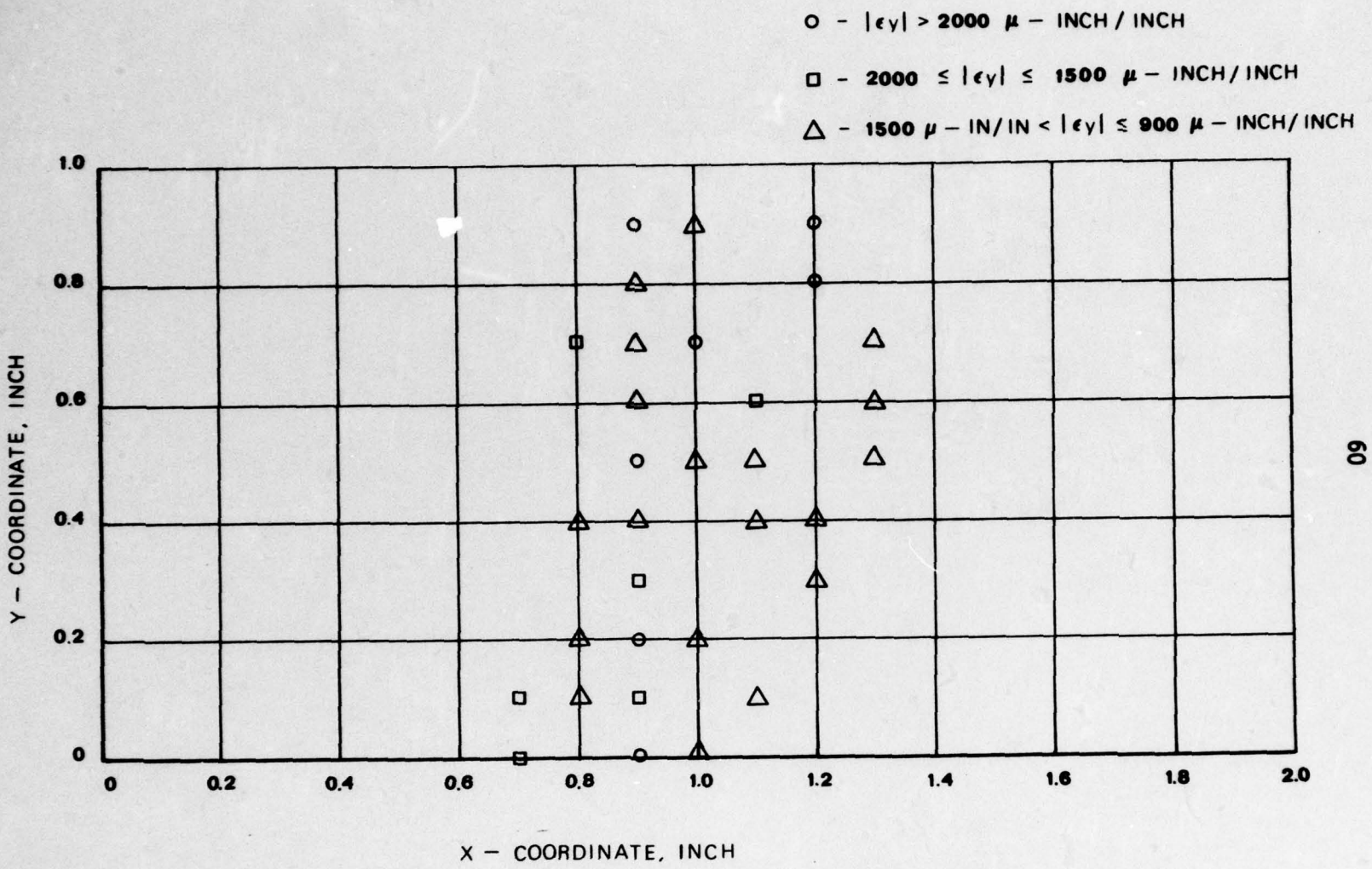

Figure 3-19. Strain Distribution for Longitudinal Flaw Cylinder

in Fig. 3-20 are shown in Figs 3-21 thru 25.

The results of the spot flaw displacements note 0 to 400 micro inches in unflawed regions. In the vicinity of the flaw (see graphs in the neighborhood of x =.8 thru 1.1 inches and y =1.1 thru 1.6 inches) the displacements change abruptly indicating high strain. Fig. 3-5 illustrated how the fringes change. Fig. 3-12 shows strain values in the direction of the cylinder axis (normal strain on an area perpendicular to the y axis) that are larger than 2000 (10^{-6}) in/in. The flaw size and location is evident. Similar results are shown in Figs. 3-19 and 3-25 for the longitudinal and circumferential flaw.

Because of the minimum stability problems (incomparison with holography and correlation fringe techniques) and because of the ease of quantitizing the results in comparison with holography, correlation fringe, shearing speckle interfereometry, and single beam speckle techniques this technique of Young's fringes is a most promising method of flaw detection.

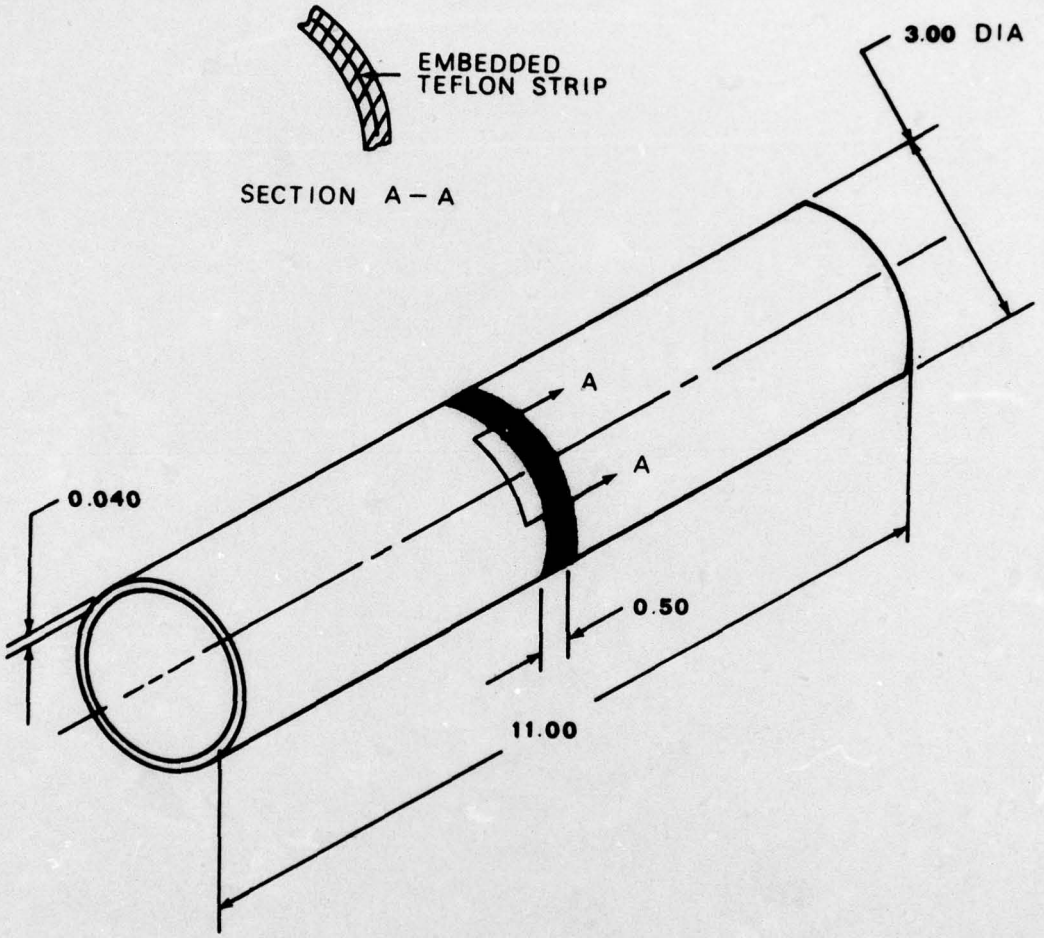

Figure 3-20. Circumferential Flaw

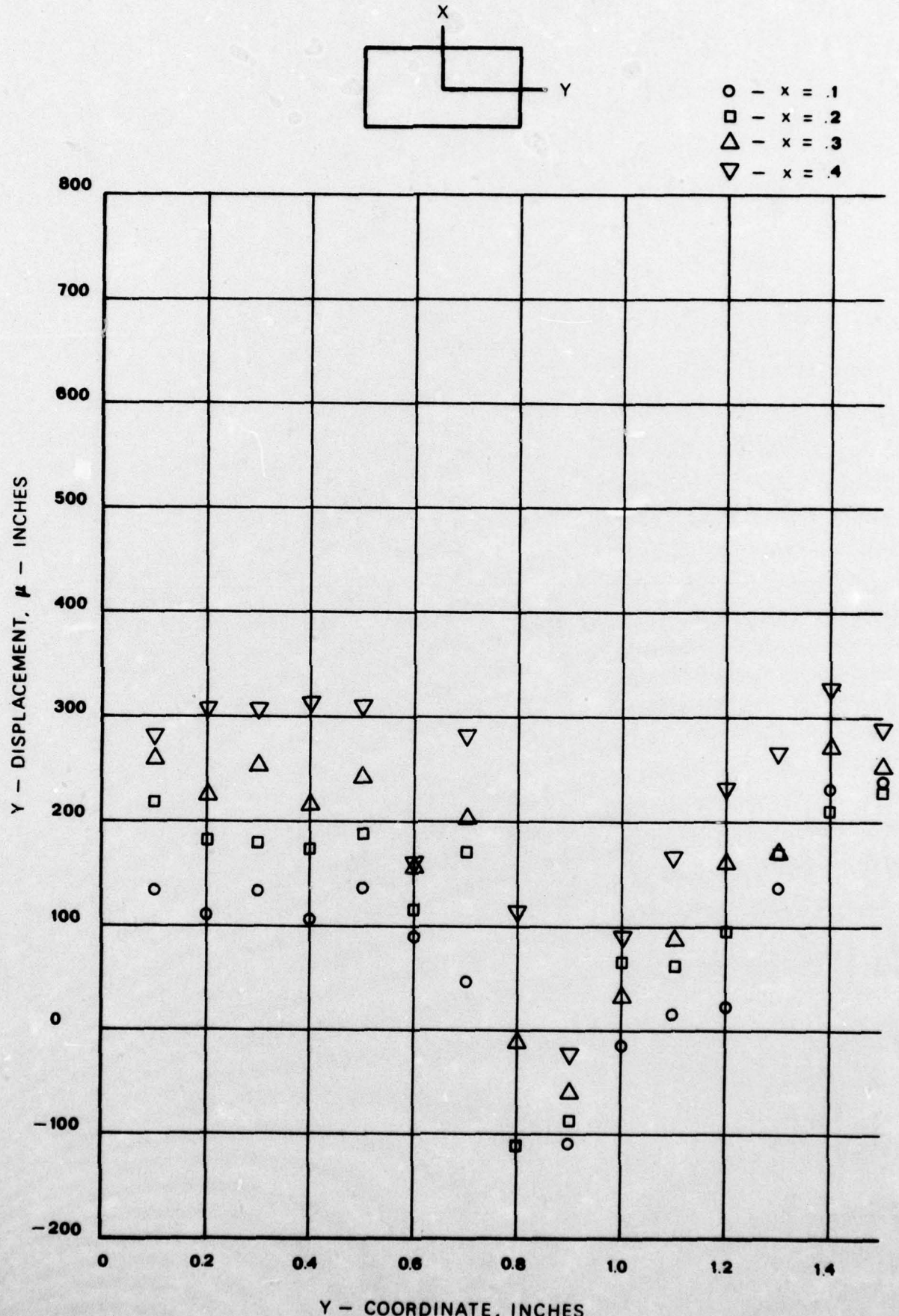

Figure 3-21. y-Displacement as a Function of y-Coordinate for Circumferential Flaw (x=0.1 - x=0.4)

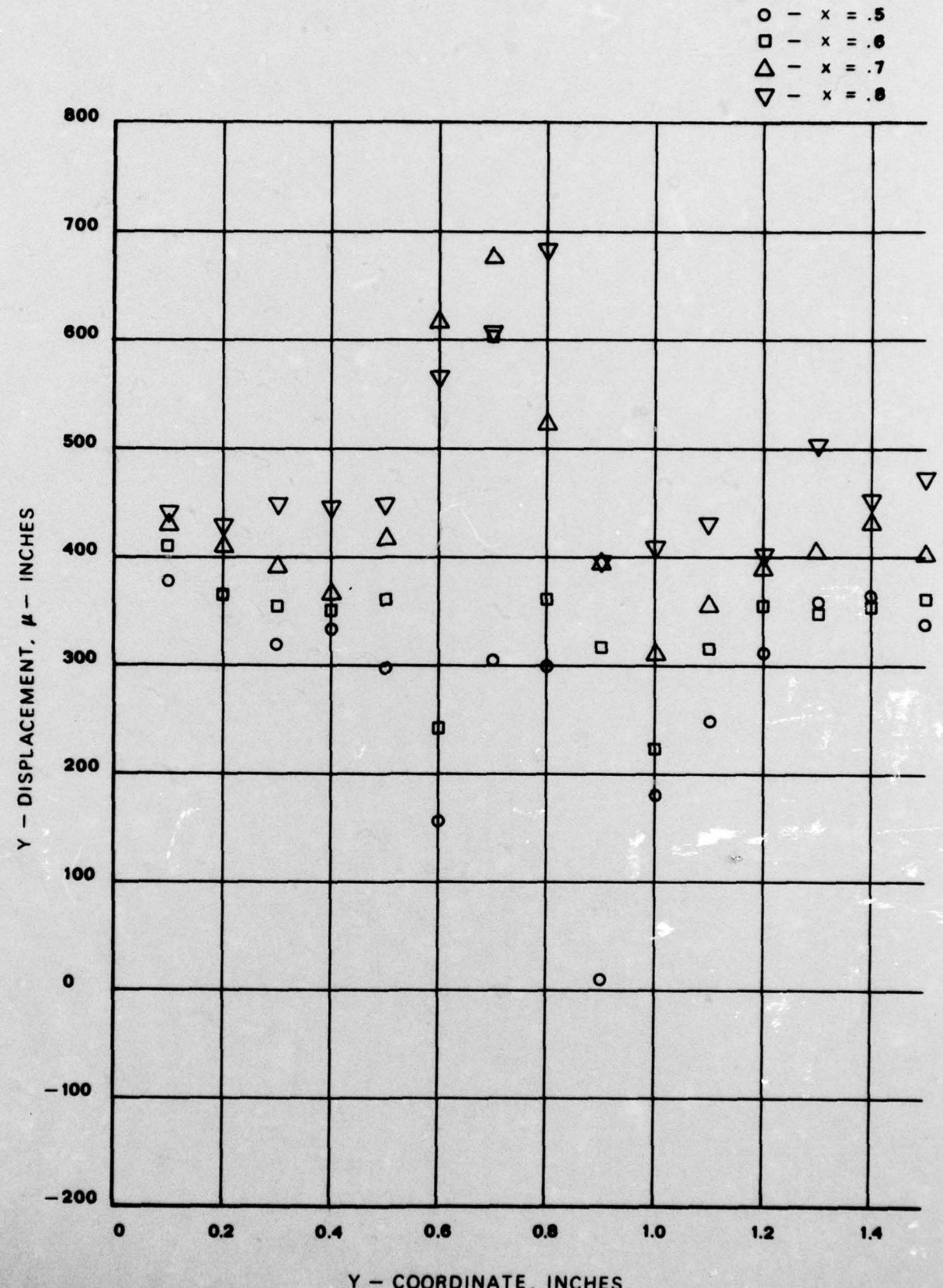

Figure 3-22. y-Displacement as a Function of y-Coordinate for Circumferential Flaw (x=0.5 - x=0.8)

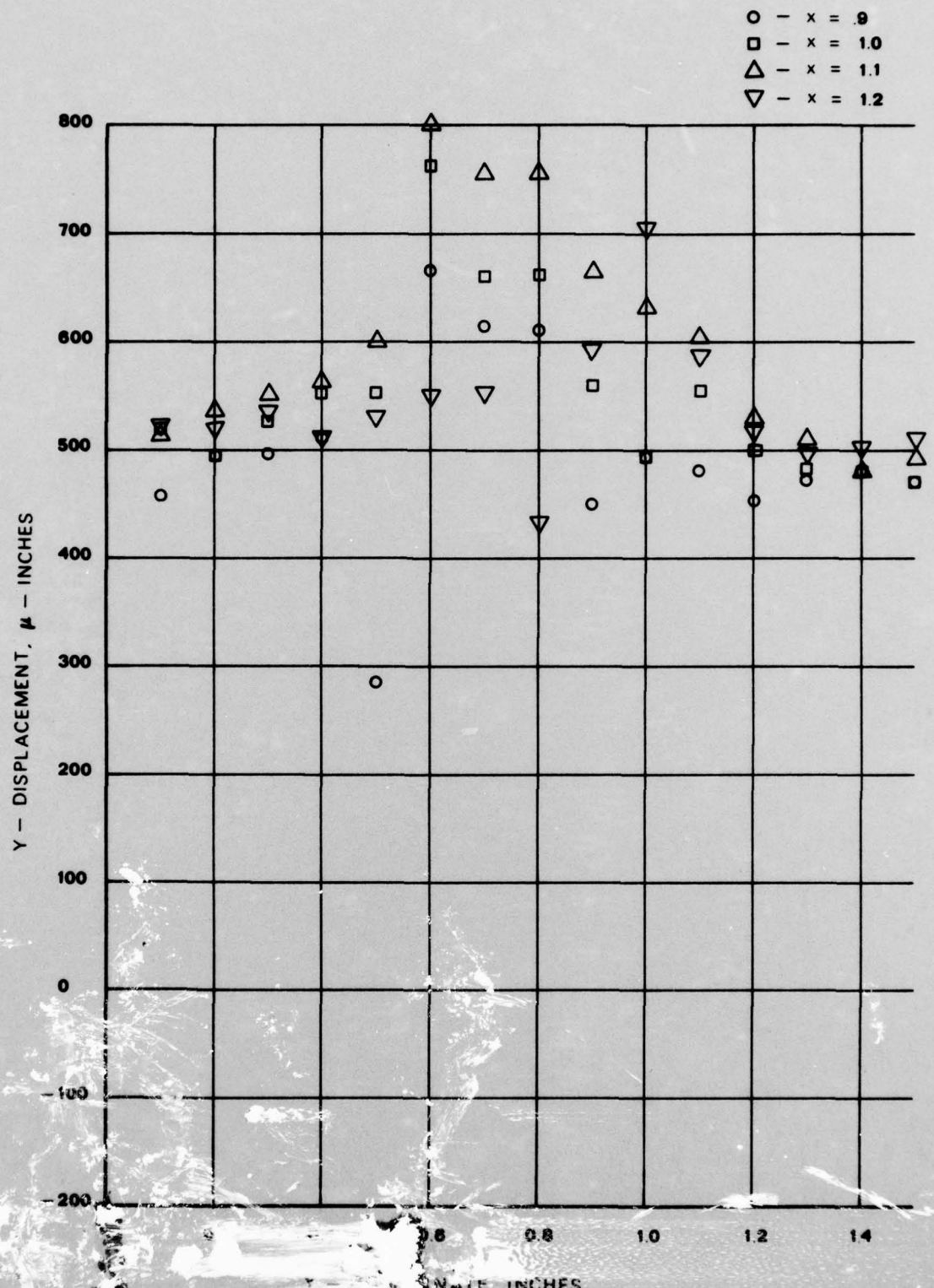

Figure 3-23. Displacement as a Function of Coordinate for Circumferential Flaw -0.9

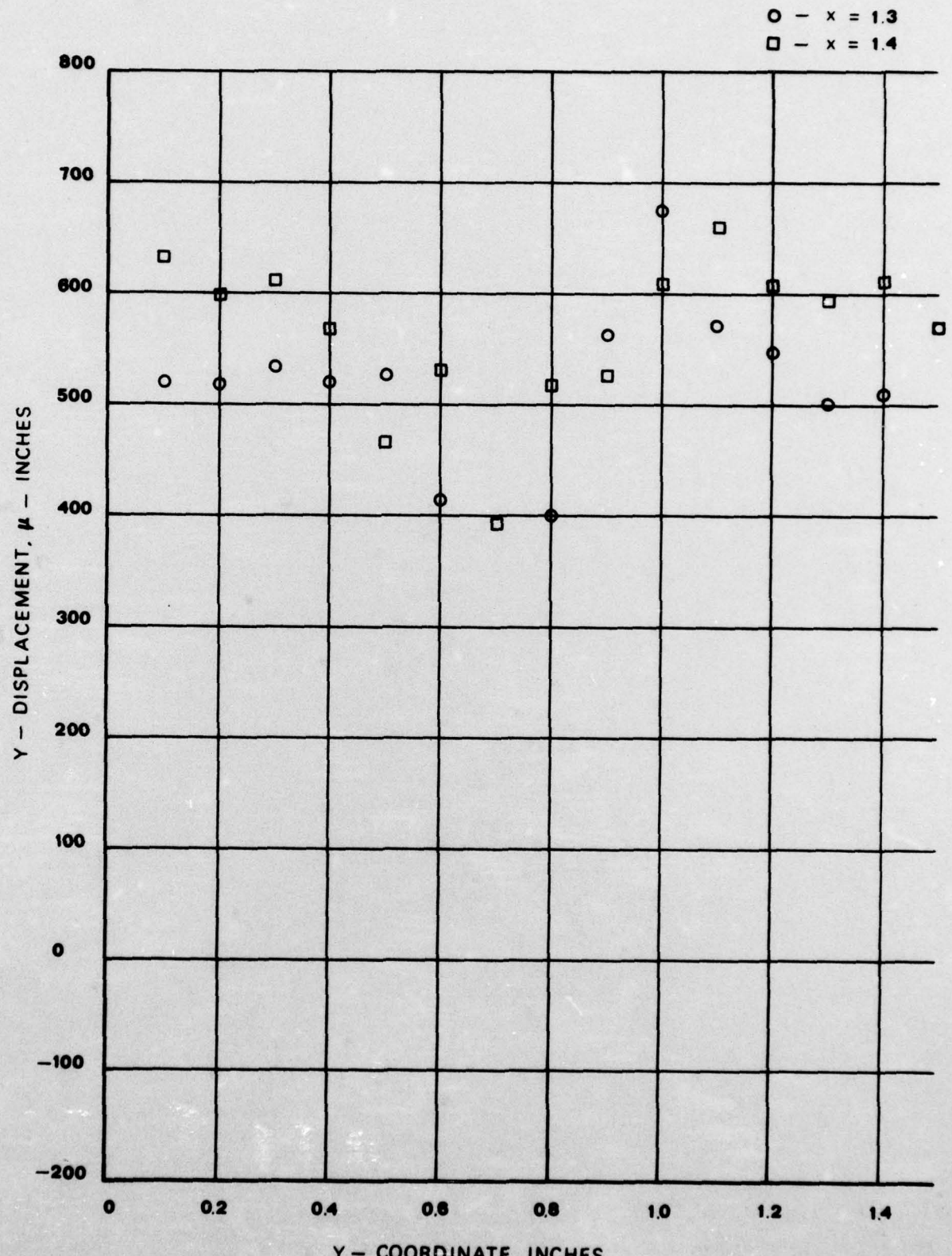

Figure 3-24. y-Displacement as a Function of y-Coordinate for Circumferential Flaw (x=1.3 - x=1.4)

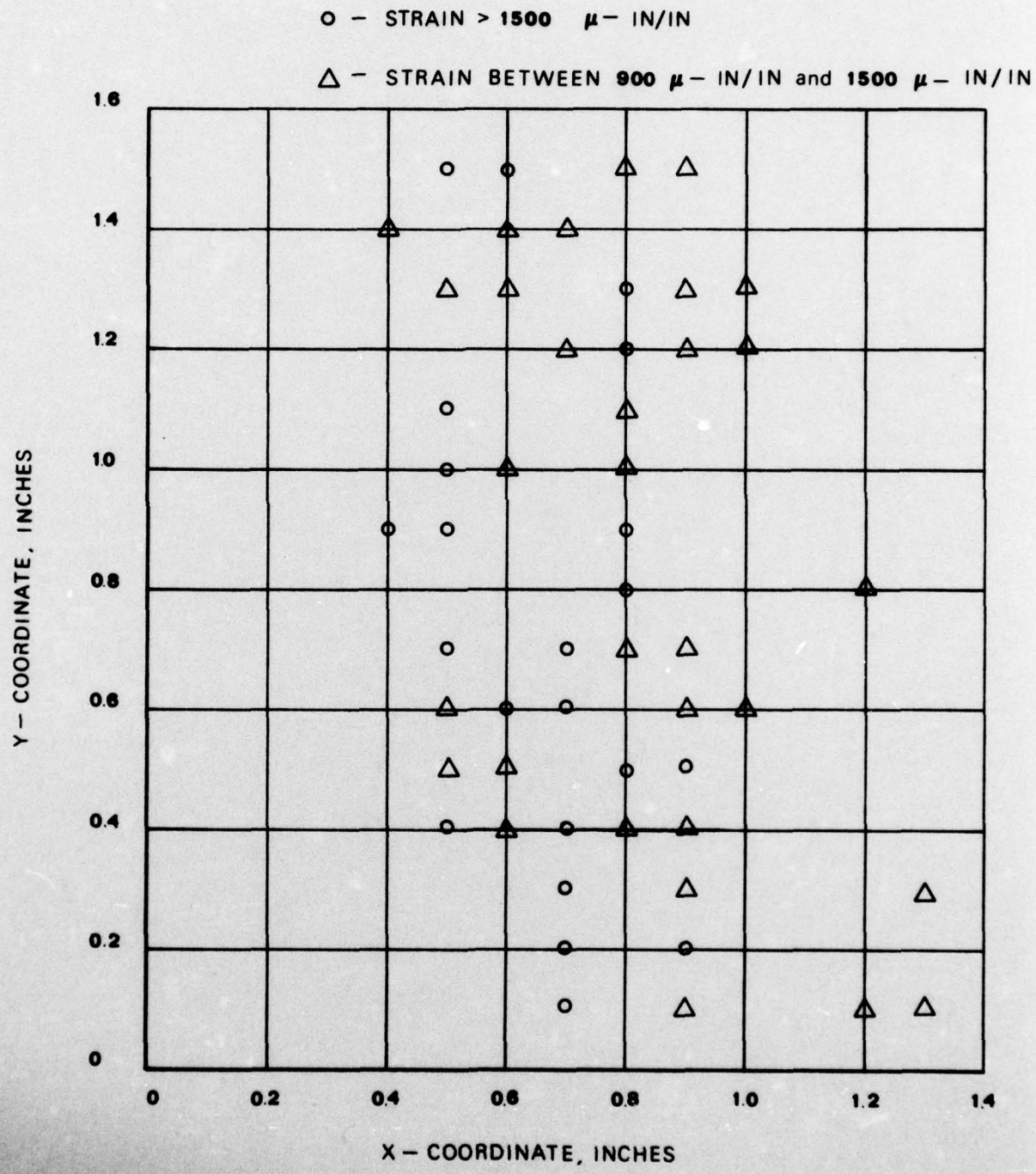

Figure 3-25. Strain Distribution for Circumferential Flaw Cylinder

SECURITY CLASSIFICATION OF THIS PAGE (When Data Entered)

REPORT DOCUMENTATION PAGE

READ INSTRUCTIONS BEFORE COMPLETING FORM

(14) 1. REPORT NUMBER: ME-AMC-0467 (Flaw)

2. GOVT ACCESSION NO.

(9) 3. RECIPIENT'S CATALOG NUMBER

(6) 4. TITLE (and Subtitle): Techniques For Flaw Detection In Composite Material Structures,

5. TYPE OF REPORT & PERIOD COVERED: Final Report, Dec 75-Dec 76

6. PERFORMING ORG. REPORT NUMBER

(10) 7. AUTHOR(s): W. F. Ranson, W. F. Swinson

8. CONTRACT OR GRANT NUMBER(s): new DAAHo1-76-C-0467

9. PERFORMING ORGANIZATION NAME AND ADDRESS: Auburn University, Engineering Experiment Station, Auburn, Alabama 36830

10. PROGRAM ELEMENT, PROJECT, TASK AREA & WORK UNIT NUMBERS

11. CONTROLLING OFFICE NAME AND ADDRESS: Headquarter, U. S. Army Missile Command, Attn: AMSMI: IPBE/SHARP, Redstone Arsenal, Al 35809

(11) 12. REPORT DATE: Dec 1976

13. NUMBER OF PAGES: 67

14. MONITORING AGENCY NAME & ADDRESS (if different from Controlling Office)

(12) 75p.

15. SECURITY CLASS. (of this report): unclassified

15a. DECLASSIFICATION/DOWNGRADING SCHEDULE

16. DISTRIBUTION STATEMENT (of this Report): unlimited (15) DAAHØ1-76-C-Ø467

17. DISTRIBUTION STATEMENT (of the abstract entered in Block 20, if different from Report)

18. SUPPLEMENTARY NOTES

19. KEY WORDS (Continue on reverse side if necessary and identify by block number)

Shearing Speckle Interferometry,
Double Exposure Speckle Photography Diffraction

20. ABSTRACT (Continue on reverse side if necessary and identify by block number)

This study concerns the nondestructive detection and quantification of flaws and voids in thin, cylindrical, fiber reinforced, composite, structures. Three types of flaws were investigated using shearing speckle and single beam speckle interferometry. The theory for each technique and photographs of the fringe patterns are presented. The Young's fringe method of speckle interferometry was used to determine the surface strains in the flaw region and the resulting flaw geometry was presented in graphical form. Shearing speckle —→ rept page

DD FORM 1 JAN 73 1473 EDITION OF 1 NOV 65 IS OBSOLETE
S/N 0102-014-6601 |

SECURITY CLASSIFICATION OF THIS PAGE (When Data Entered)

402 958

4/B

20. interferometry was developed for a qualitative analysis only.
The results show that flaws in their fiber reinforced composite structures can be detected and the size determined by either shearing speckle or single beam speckle interferometry.